iScience

CellPress
OPEN ACCESS

Article

Sequential Wnt Agonist Then Antagonist Treatment Accelerates Tissue Repair and Minimizes Fibrosis

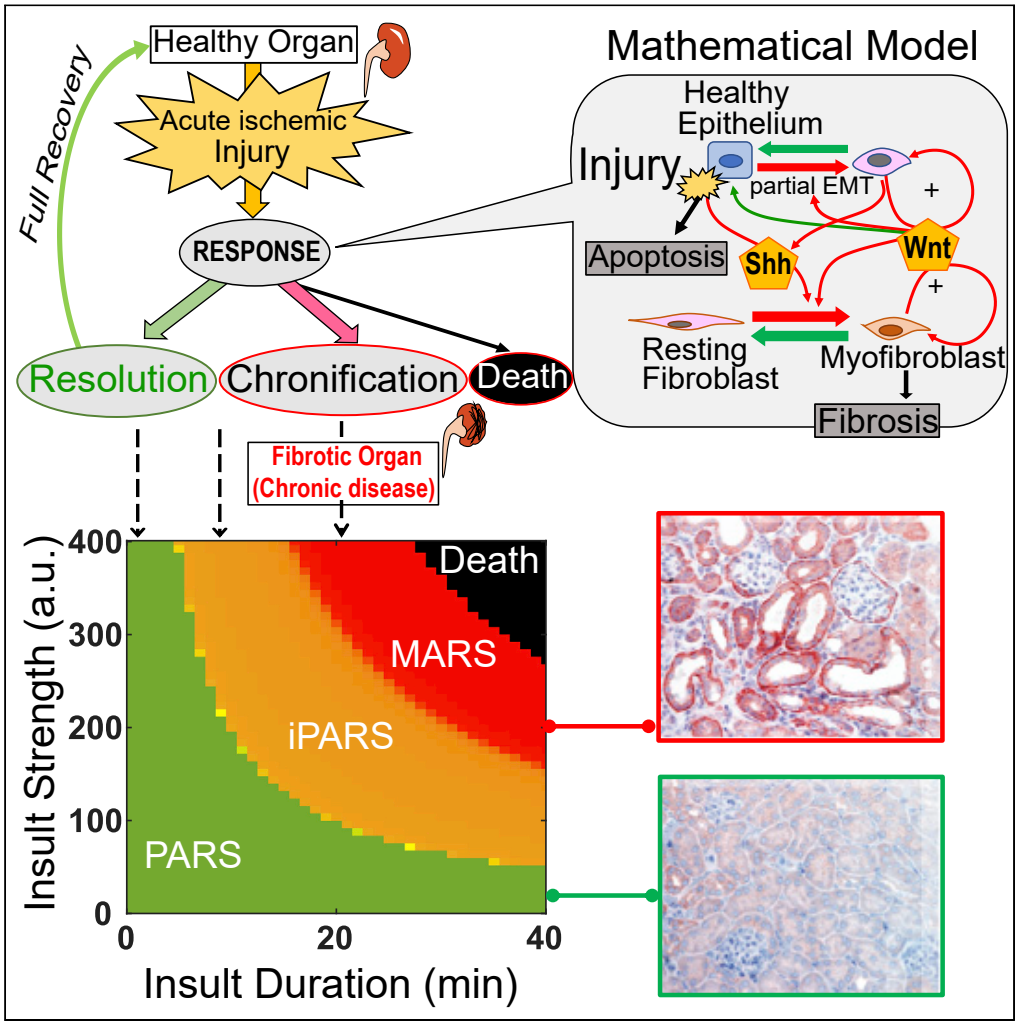

Xiao-Jun Tian, Dong Zhou, Haiyan Fu, ..., Sui Huang, Youhua Liu, Jianhua Xing

xiaojun.tian@asu.edu (X.-J.T.)
yhliu@pitt.edu (Y.L.)
xing1@pitt.edu (J.X.)

HIGHLIGHTS

Quick repair and complete resolution are incompatible requirements for AKI repair

Four discrete terminal states are revealed depending on the duration of ischemia

Imperfective adaptive response state reduces death risk but increases CKD risk

Sequential combination therapy was effective in reducing both death and fibrosis

Tian et al., iScience *23*, 101047
May 22, 2020 © 2020 The Author(s).
https://doi.org/10.1016/j.isci.2020.101047

iScience

CellPress
OPEN ACCESS

Article

Sequential Wnt Agonist Then Antagonist Treatment Accelerates Tissue Repair and Minimizes Fibrosis

Xiao-Jun Tian,[1,2,8,*] Dong Zhou,[3,8] Haiyan Fu,[4,8] Rong Zhang,[2] Xiaojie Wang,[3] Sui Huang,[5] Youhua Liu,[3,4,*] and Jianhua Xing[1,6,7,9,*]

SUMMARY

Tissue fibrosis compromises organ function and occurs as a potential long-term outcome in response to acute tissue injuries. Currently, lack of mechanistic understanding prevents effective prevention and treatment of the progression from acute injury to fibrosis. Here, we combined quantitative experimental studies with a mouse kidney injury model and a computational approach to determine how the physiological consequences are determined by the severity of ischemia injury and to identify how to manipulate Wnt signaling to accelerate repair of ischemic tissue damage while minimizing fibrosis. The study reveals that memory of prior injury contributes to fibrosis progression and ischemic preconditioning reduces the risk of death but increases the risk of fibrosis. Furthermore, we validated the prediction that sequential combination therapy of initial treatment with a Wnt agonist followed by treatment with a Wnt antagonist can reduce both the risk of death and fibrosis in response to acute injuries.

INTRODUCTION

Acute injury of organs triggers inflammation and wound healing to restore tissue integrity and function. This rapid repair response involves a complex cascade of inflammatory processes that contain the damage and trigger regeneration (Koh and DiPietro, 2011; Wynn, 2008). During this response, instead of the signaling pathways that maintain tissue homeostasis, pathways that control self-propelling yet self-limiting program are active. During the tissue healing response, many diverse cell types, both resident and infiltrating cells, communicate through secreted signals and cell contact to modulate each other's behaviors. Some of these behaviors include proliferation and transitions between different cellular states, such as differentiated cells adopting a transient progenitor-like state or quiescent stem cells adopting an activated state (Wynn, 2008). A critical phase in the repair process is the resolution (Serhan et al., 2007), which terminates inflammation and regeneration once the damaged tissue is repaired: excess cells die, return to quiescence, or re-differentiate.

Perfect repair of injury is not always possible, especially when large areas of damage or repeated injuries occur. Consequently, the resolution process is altered resulting in the formation of scars or tissue fibrosis. In some cases, such as chronic kidney disease (CKD) (Humphreys, 2018), chronic progressive fibrosis occurs (Gardet et al., 2013) due to excess proliferation of fibroblasts and deposition of the extracellular matrix. Chronic progressive fibrosis impairs organ function and can ultimately lead to organ failure and death. Chronic progressive fibrosis is not simply "incomplete" or "altered" repair; instead, it results from excessive repair activity and failure of resolution and is, thus, a maladaptive response. Fibrosis impairs organ function in heart, kidney, and liver diseases and is a complication that impairs function after organ transplantation and organ health following surgery. For example, ischemic kidney injury is a common consequence of cardiac surgery (O'Neal et al., 2016).

Here, we used a mouse model of ischemic kidney injury to explore acute injury repair and chronic fibrosis. Exposure to toxins or hypoxic stress can lead to loss of epithelial cells in the renal tubules, causing either acute kidney injury (AKI) with kidney failure or CKD that progresses irreversibly to end-stage renal insufficiency. AKI and CKD are global health challenges with limited treatment options (Wynn and Ramalingam, 2012). These two conditions are often mechanistically and clinically linked (Belayev and Palevsky, 2014;

[1]Department of Computational and Systems Biology, School of Medicine, University of Pittsburgh, 3501 Fifth Avenue, Pittsburgh, PA 15261, USA

[2]School of Biological and Health Systems Engineering, Arizona State University, Tempe, AZ 85287, USA

[3]Department of Pathology, School of Medicine, University of Pittsburgh, 200 Lothrop Street, Pittsburgh, PA 15261, USA

[4]State Key Laboratory of Organ Failure Research, National Clinical Research Center of Kidney Disease, Division of Nephrology, Nanfang Hospital, Southern Medical University, Guangzhou 510515, China

[5]Institute for Systems Biology, Seattle, WA, USA

[6]Department of Physics, University of Pittsburgh, Pittsburgh, PA 15261, USA

[7]UPMC-Hillman Cancer Center, University of Pittsburgh, Pittsburgh, PA 15232, USA

[8]These authors contributed equally

[9]Lead Contact

*Correspondence: xiaojun.tian@asu.edu (X.-J.T.), yhliu@pitt.edu (Y.L.), xing1@pitt.edu (J.X.)

https://doi.org/10.1016/j.isci.2020.101047

This is an open access article under the CC BY-NC-ND license (http://creativecommons.org/licenses/by-nc-nd/4.0/).

Ferenbach and Bonventre, 2015; Leung et al., 2013). Although some patients completely recover from AKI, others progress to CKD (Amdur et al., 2009; Coca et al., 2009). The determining factors for the transition from AKI to CKD are not clear. The risk of CKD increases if a patient survives a single episode of AKI and further increases with repetitive AKI episodes (Chawla and Kimmel, 2012; Coca et al., 2012). In mice, exposing the kidney to mild ischemia prior to injury (ischemic preconditioning) protects against renal damage from a subsequent AKI (Bonventre, 2002; Joo et al., 2006; Park et al., 2001). Clinical trials of ischemic preconditioning for AKI associated with cardiac surgery are ongoing (Li et al., 2017; Zarbock et al., 2015).

Mechanistically, kidney tissue injury stimulates two connected cellular networks (tubular cells and fibroblasts) through signals mediated by the Sonic hedgehog (Shh) and Wnt pathways. Shh released by the kidney tubular cells stimulates the proliferation of activated fibroblasts to promote tissue repair (Zhou et al., 2014). Wnt produced by both tubular cells and fibroblasts participates in both repair of injured tissue and stimulation of fibrosis (Akhmetshina et al., 2012; Wang et al., 2018; Xiao et al., 2016; Zhou et al., 2016). In particular, Wnt signaling stimulates cell state transitions, including epithelial-to-mesenchymal transition (EMT) and partial EMT (pEMT), which contribute to both tissue repair and many chronic fibrotic diseases (Humphreys, 2018; Tennakoon et al., 2016; Willis et al., 2005). After AKI, some kidney tubular epithelial cells undergo pEMT and some activated fibroblasts become myofibroblasts, the latter of which is a critical event in the development of fibrosis (Grande et al., 2015; Lovisa et al., 2015). The Wnt-stimulated process of myofibroblast expansion could serve as a drug target for limiting fibrosis and development of CKD. Consistent with this hypothesis, excessive and prolonged activation of Wnt signaling promotes myofibroblast proliferation and fibrogenesis and correlates with progression to CKD (Xiao et al., 2016; Zhou et al., 2016).

The apparent seemingly contradiction of the beneficial effects of ischemic preconditioning and the established detrimental role of Wnt activation on fibrosis development has led to a long-standing puzzle in the field of AKI and CKD studies. To resolve this controversy, here we combined quantitative experimental studies with a mouse kidney injury model and a nonlinear dynamical systems model of the cellular interaction network composed of a tubular epithelial cell module and a fibroblast cell module, involving three cell states in each module, and regulatory signals mediated by Shh and Wnt. We used this cellular network model to investigate the transition from acute injury and repair to chronic tissue damage and fibrosis. The model provided a mechanism for the multiple outcomes of kidney injury found experimentally in a mouse model. Furthermore, the model predicted a potential increased risk of fibrosis of ischemic preconditioning despite its well-known protective effect, which was validated in a mouse kidney ischemia system. Importantly, we developed a Wnt pathway-targeted treatment regimen involving sequential agonist then antagonist treatment to accelerate tissue repair and prevent fibrosis with the guidance of computational multi-objective optimization. These findings are particularly relevant in the context of surgery when the timing of the ischemic episode is known and treatments can be initiated and strategically planned to optimize positive outcomes.

RESULTS

Mouse Models Reveal Four Discrete Terminal States Depending on the Duration of Acute Kidney Injuries

We established a mouse model for AKI (the ischemia-reperfusion injury [IRI] model) to study whether varying a single input variable (the severity of transient ischemia) produces qualitatively distinct repair outcomes. If so, then the system is a complex non-linear dynamical system, which has the property that multiple distinct stable outcomes arise in response to a continuous range of a perturbation. We tuned the severity of kidney injury by varying the duration of ischemia (Xiao et al., 2016): mild (5 min), moderate (10, 15, and 20 min), and severe (30 min) IRI. All mice exposed to mild IRI survived, four of seven mice exposed to each of the moderate IRI conditions survived, and only six of sixteen mice exposed to severe IRI survived. Surviving mice recovered for 30 days; then we analyzed the kidney tissue by periodic acid-Schiff (PAS) (Figure S1) to evaluate the severity of injury based on morphological changes and marker expressions. We stained for Wnt1, Vimentin, fibroblast specific protein 1 (FSP-1), α-smooth muscle actin (α-SMA), and platelet-derived growth factor receptor-β (PDGFR-β) by immunohistochemistry to monitor the activation of fibroblasts and pEMT (Figures 1A and 1B). For animals subjected to mild IRI, we observed that all markers returned to basal levels like those in control mice not exposed to IRI. The response to 10-min IRI was more variable: some mice had a small but statistically significant increase in Wnt1, FSP-1, and vimentin, but not PDGFR-β; only one mouse had a statistically significant increase in α-SMA. The other

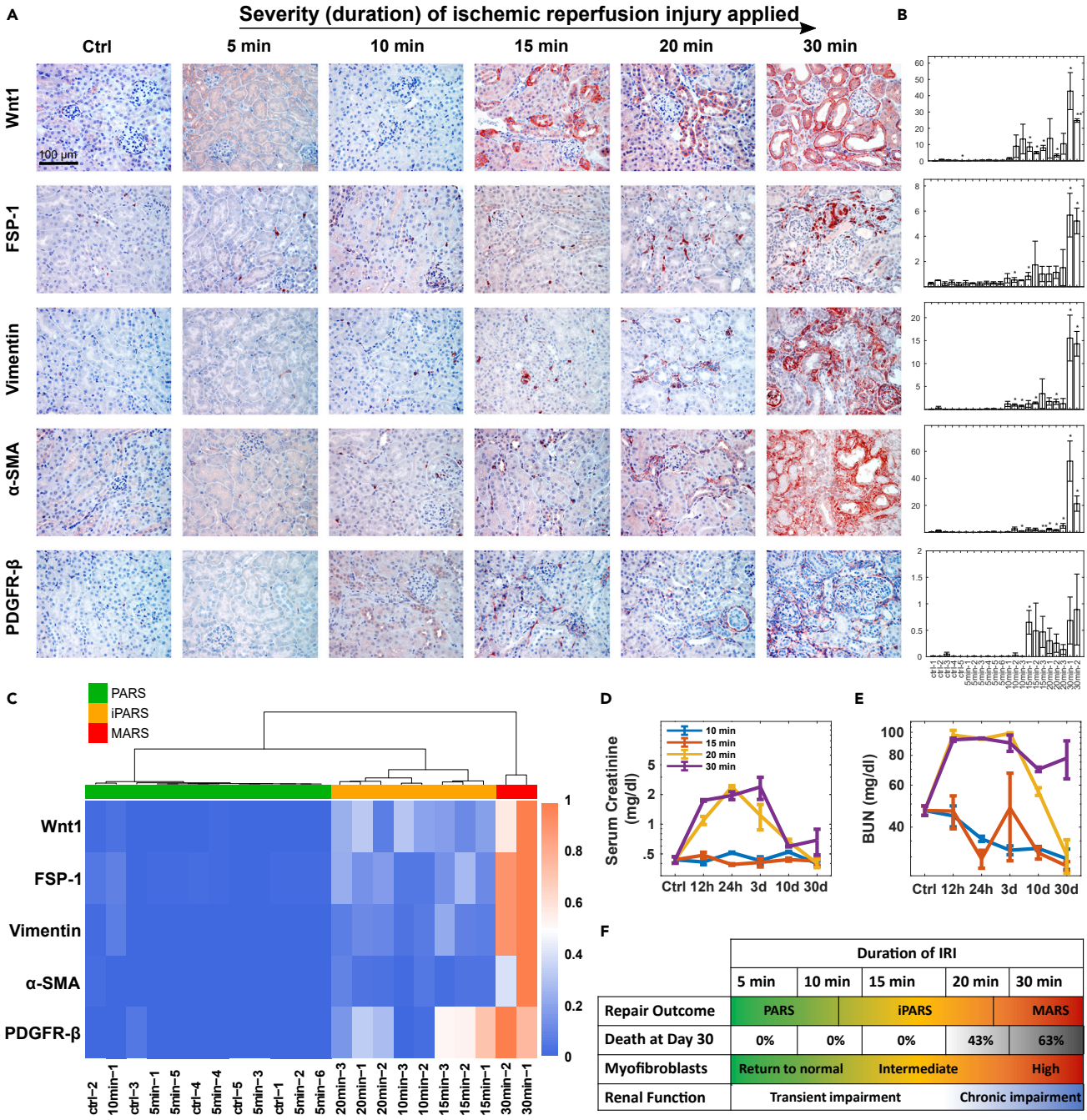

Figure 1. Mouse Models Show the Existence of Four Possible Outcomes Depending on the Duration of Acute Kidney Injuries

(A) Representative micrographs showing expression of Wnt1, FSP-1, Vimentin, α-SMA, and PDGFR-β in control and diseased kidneys 30 days after varying degrees of IRI. Scale bar, 100 μm.

(B) Quantification of marker levels. Each column indicates an individual mouse. Data are represented as mean ± SEM of three slices for each marker each mouse. $^{**}p < 0.005$, $^{*}p < 0.05$ versus control using t test (n = 5).

(C) Hierarchical clustering analysis of the marker levels on day 30 after different duration of IRI treatment.

(D and E) Temporal profiles of renal function markers, serum creatinine (D) and BUN (E) after various duration of IRI. n = 3, Data are represented as mean ± SEM.

(F) The fraction of the dead mice, repair outcomes, myofibroblast expansion, and renal function depends on the duration of IRI.

See also Figure S1.

three experimental groups displayed a significant increase in all five markers. Mice exposed to the severe IRI displayed the highest amounts of all of these markers and had large fibrotic patches (Figures 1A and S1). In contrast, small and scattered fibrotic patches were observed in mice after 15- or 20-min IRI (Figure S1).

Cluster analysis with these markers 30 days after injury divided the surviving mice into three readily distinguishable groups (Figure 1C) representing the treatment groups, indicating that these markers adequately captured the differences between the mild, moderate, and severe injury conditions. In the mice in the 5-min IRI group, the markers returned to basal, the tissue was morphologically indistinguishable from the control mice, and the mice clustered with the control mice, indicating that the repair response was complete and resolved. Hence, we defined the kidney tissue state in the mice of this cluster as a "perfect adaptive response state" (PARS). The markers of mice in the 15- and 20-min IRI groups indicated the persistence of low levels of Wnt and low numbers of residual activated fibroblasts and pEMT cells; thus, we defined this as an "imperfect adaptive response state" (iPARS). The third cluster of the 30-min IRI group had kidneys with high amounts of Wnt and markers of myofibroblasts and pEMT cells; thus, we defined this as a "maladaptive response state" (MARS).

To determine how increasing the severity of IRI affected kidney function, we evaluated kidney function based on serum creatinine and blood urea nitrogen (BUN), which are routinely used to assess kidney function in patients. By 30 days after IRI, only the mice in the severe IRI group exhibited compromised kidney function (Figures 1D and 1E). Consistent with the severe IRI and 20-min moderate IRI group exhibiting the most impairment in kidney function (highest serum creatinine and BUN), several animals died in those two groups of mice in the first 2 weeks after the IRI (Figure 1F).

These data suggest that the kidney response to IRI is a complex non-linear dynamical system. A single quantitative variable, the duration of ischemia, produced four qualitatively distinct outcomes: (1) full adaptive recovery (PARS), (2) imperfect recovery with mild lasting tissue changes but restored kidney function (iPARS), (3) a maladaptive response (MARS) with signs of fibrosis and renal dysfunction, and (4) death.

A Mathematical Model of the Regulatory Network of the Kidney Response to Injury Accurately Recapitulates the Four Observed Outcomes

We first asked whether the four distinct and robustly separable outcomes in the animals, triggered by varying the magnitude of one experimentally controllable parameter, reflect inherent dynamical behaviors of the cell-cell interaction network that orchestrates the repair response. We constructed a canonical model with the key components involved in kidney repair (Figure 2A, Tables S1 and S2). We represented the model with ordinary differential equations with eight variables representing the rates of change in the abundance of cells and the two signaling mediators (Shh, Wnt) (Supplemental Information). The cellular components of the network are represented by two modules: the tubular module (representing the tubular epithelial cells) and the fibroblast module, each containing three distinct cell states. Shh and Wnt produced by the cells in the cellular modules mediate the interactions between the two modules. The cells proliferate, undergo state transitions, or die under the influence of these two signaling molecules in response to ischemic injury ("insult" in the model). The outcome variables include (1) the fraction of dead tubular epithelial cells (Figure S2A, see Supplemental Information: The fate of organism death in the mathematical model) and (2) the abundance of myofibroblasts. We selected the number of myofibroblasts as a determinant of the outcome related to fibrosis, because the abundance of myofibroblasts is a major determinant of this pathology through secreting extracellular matrix (ECM) (LeBleu et al., 2013). Thus, the effect of ECM is implicated included in the model based on a positive correlation between the number of fibroblasts and ECM. Using these variables, we set to examine whether the system could reproduce multiple clinically and experimentally observed outcomes, such as full recovery without fibrosis (no dead tubular epithelial cells and no increase in myofibroblasts compared with the uninjured state), fibrosis (indicated by the steady-state abundance of myofibroblasts), or organismal death (modeled as the number of dead tubular epithelial cells exceeding a preset threshold).

Under physiological conditions, the number of fibroblasts residing in the interstitial compartment is low (Lovisa et al., 2015). We model these as "resident fibroblasts" (Figure 2A). In response to insult, some healthy epithelial cells ("tubular epithelium" in the model) enter the injured state ("injured tubular cells") and promote self-renewal of neighboring tubular epithelial cells. In the model, Shh promotes resident fibroblasts to transition into the state "activated fibroblast" in which they proliferate and from which they

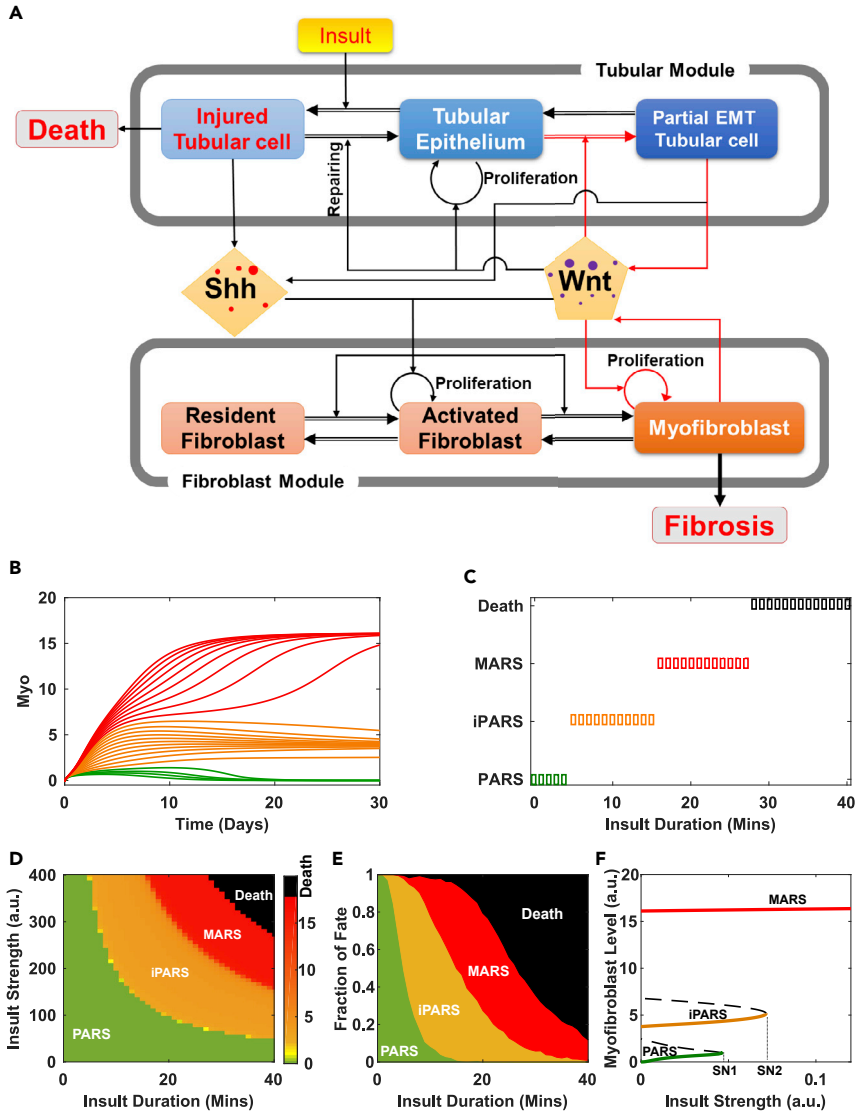

Figure 2. Theoretical Analyses Reveal the Mechanism of the Four Outcomes in Response to Renal Injury

(A) Cell-cell communication model for renal homeostasis and fibrosis. The positive feedback loops are highlighted in red.

(B) Simulated time series of the number of myofibroblasts under different durations of insult.

(C) Repair outcomes under insult of fixed strength but increasing durations.

(D) Phase diagram of repair outcomes (indicated by myofibroblast level) in the space of insult strength and duration.

(E) Fraction of outcomes as a function of insult duration sampled from 1,000 independent simulations.

(F) Bifurcation diagram of the myofibroblast level with respect to insult strength shows three possible survival outcomes depending on the strength of the insult.

See also Figure S2 and Tables S1 and S2.

can further transition into the state "myofibroblast" (Grgic et al., 2012; Zhou et al., 2014). The myofibroblasts secrete Wnt, which stimulates the proliferation of both activated fibroblasts and myofibroblasts, establishing a positive feedback loop between the myofibroblasts and Wnt production.

Wnt also affects the tubular module (Lyons et al., 2004), further promoting self-renewal and repair of injured tubular epithelial cells. Wnt also stimulates tubular epithelial cells to undergo a state transition to pEMT ("partial EMT tubular cell") (Grande et al., 2015; Kusaba et al., 2014; Lovisa et al., 2015; Yang et al., 2010; Zhou et al., 2016), which also secretes Wnt (Grande et al., 2015). This establishes a second positive feedback loop between the partial EMT tubular cell and Wnt production.

To determine the outcomes produced by the model, we set the parameters to those for mice (see Tables S1 and S2 for values of parameters and initial states, see Supplemental Information: Parameter Estimation and Justification), then monitored the distinct stable steady states produced by the model as a function of myofibroblast number by either applying a range of insult intensities (Figure 2B) or starting from a range of initial conditions (Figure S2B). The simulated time course of the number of myofibroblasts showed that the network existed in one of three stable steady states with respect to myofibroblast abundance: return to baseline, persistent intermediate numbers of myofibroblasts, or persistent high numbers of myofibroblasts (Figures 2B and S2B). Increasing insult duration and incorporating the number of dead tubular epithelial cells into the outcome of the model resulted in the separation of organismal death from states associated with survival and separated each of the three survival-associated steady states into those representing severe fibrosis associated with high numbers of myofibroblasts (representing MARS in the mouse experiments), low numbers of residual myofibroblasts (representing iPARS), and no fibrosis, no increase in myofibroblasts from baseline, and complete recovery of tubular epithelial cells (representing PARS) (Figure 2C). Further analysis of the cell network (Figure S2C) suggested that the three steady states associated with survival are stable with respect to other system variables.

Consequently, we could parameterize insult by duration and strength in a 2D-phase diagram, which is divided into the four outcome domains and revealed that a short and severe insult had a similar effect as a longer but less severe one (Figure 2D). To account for the stochastic variability between mice, we simulated an ensemble of models with parameters randomly and uniformly chosen within $\pm$20% of its default value and measured the fraction of mice exhibiting each of the four outcomes. By representing the data on a 2D-phase diagram, we showed that the fraction of mice displaying PARS decreased with increasing duration of the insult and that the fraction of mice suffering from the next higher-level severity of disease (or death) increased with increasing duration of the insult (Figure 2E). This outcome is consistent with the experimental results observed for the mice (Figure 1F).

Bifurcation Analysis Reveals Increasing Insult Severity Triggers Distinct Irreversible States

Because the three outcomes—PARS, iPARS, and MARS—map to stable steady states of the cellular network model (Figure 2A), we performed an analysis of the irreversibility of the states using one-parameter bifurcation analysis. Under mild insult, the system ended in PARS (Figure 2F, green line) and returned to the state prior to the insult after removing the insult (with zero myofibroblasts at zero insult strength). However, increasing insult severity above a threshold (Figure 2F, SN1) resulted in the system crossing a first bifurcation point. Consequently, the system "jumped" to iPARS (Figure 2F, orange line). In this state, the system exhibited hysteresis, because reducing the insult strength to zero did not restore a completely healthy tissue composition. Instead, low levels of myofibroblasts remained. This is consistent with the preservation of kidney function that we observed in the mice (Figures 1D and 1E). With further increase of insult strength beyond a second critical point (Figure 2F, SN2), the system jumped to MARS (Figure 2F, red line), characterized by high abundance of myofibroblasts that persisted even after the insult was reduced to zero. Thus, the model predicted that both iPARS and MARS are irreversible states (for full bifurcation diagram, see Figure S2D). That is, the system in iPARS and MARS has memory that persists even after the end of ischemia, represented as the remnants of tissue pathology or the progression to fibrosis. Parameter sensitivity analysis (Figure S2E) revealed that all four outcomes existed within a parameter range of 15% increase or decrease of most parameters, indicating that existence of these outcomes is insensitive to heterogeneity of individual mice or our model parameter choice.

Preconditioning to iPARS Reduces Risk of Death but Increases Risk of Fibrosis

Mild ischemic insults have a protective role against subsequent insults in several organ systems, such as brain, heart, liver, and kidney. Protective preconditioning is being explored as a therapeutic modality for kidney injury associated with cardiac surgery (Bonventre, 2002; Joo et al., 2006; Park et al., 2001). We hypothesized that mice surviving a previous AKI would be in iPARS, which would protect them against subsequent ischemic events but would increase their risk of CKD after subsequent ischemic events. We examined whether protective preconditioning is a property of our kidney cellular interaction network. We simulated a moderate renal insult (10 min) to place the system into iPARS, characterized by the absence of dead tubular cells and the presence of residual myofibroblasts (Figure 3A, solid black lines). Following a second moderate insult (15 min), the percentage of dead tubular cells reduced faster, indicating faster repair and regeneration, in the preconditioned system (Figure 3A left, red solid line) than in the control system without preconditioning (Figure 3A left, black dashed lines). Thus, our system exhibited another type of memory, i.e., a protective priming effect of preconditioning.

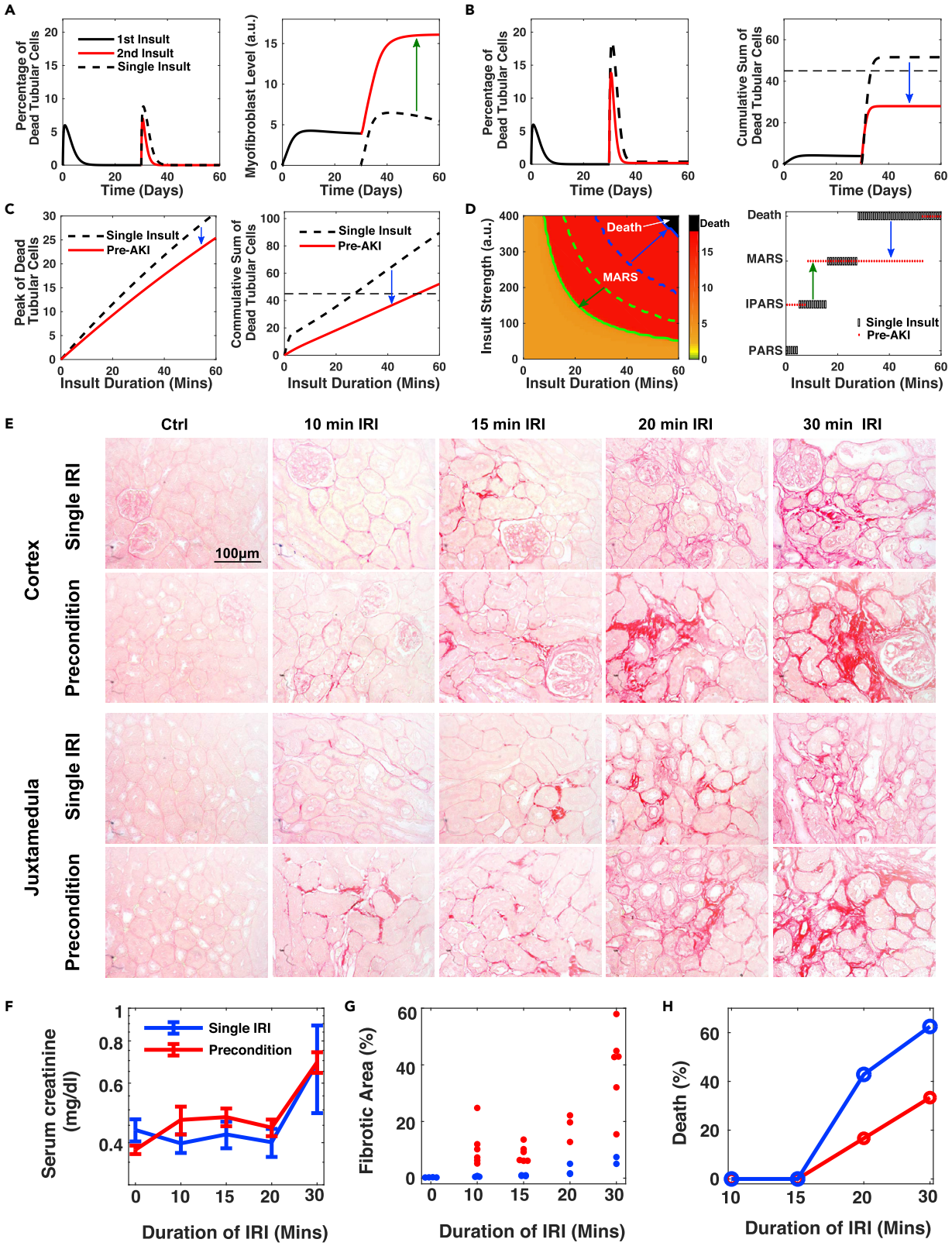
A
Percentage of Dead Tubular Cells
1st Insult
2nd Insult
Single Insult
Time (Days)
Myofibroblast Level (a.u.)
Time (Days)
B
Percentage of Dead Tubular Cells
Time (Days)
Cumulative Sum of Dead Tubular Cells
Time (Days)
C
Peak of Dead Tubular Cells
Single Insult
Pre-AKI
Insult Duration (Mins)
Commulative Sum of Dead Tubular Cells
Single Insult
Pre-AKI
Insult Duration (Mins)
D
Insult Strength (a.u.)
Death
MARS
Death
Insult Duration (Mins)
Death
MARS
IPARS
PARS
Single Insult
Pre-AKI
Insult Duration (Mins)
E
Ctrl
10 min IRI
15 min IRI
20 min IRI
30 min IRI
Cortex
Single IRI
Precondition
Juxtamedula
Single IRI
Precondition
100μm
F
Serum creatinine (mg/dl)
Single IRI
Precondition
Duration of IRI (Mins)
G
Fibrotic Area (%)
Duration of IRI (Mins)
H
Death (%)
Duration of IRI (Mins)

Figure 3. Double-Edged Sword Effects of Pre-fibrotic iPARS, Reducing the Risk of Death but Increasing the Risk of MARS

(A) Temporal profiles of the percentage of dead tubular cells and the myofibroblast level under one 10-min insult (dashed lines) and two successive insults with one second 15-min insult occurring 30 days after the first (solid lines). The green arrow indicates the change from iPARS to MARS with pretreatment.

(B) Same as (A) and (B) except with a 30-min second insult. The horizontal line indicates the threshold for death. The blue arrow indicates the change from Death to MARS with pretreatment.

(C) Peak level of dead tubular cells and maximum level of the cumulative death tubular cells as a function of insult duration. The system is either preconditioned with a first moderate insult (solid red lines) or without preconditioning (black dash lines) as control.

(D) (Left) Phase diagram of repair outcomes (indicated by myofibroblast level) in the space of insult strength and duration. Similar to Figure 2D, except preconditioned with a moderate insult (duration = 10 min, 30 days of recovery after first insult). Green lines indicate the threshold of MARS with (solid) and without (dashed) preconditioning. Blue lines indicate the threshold of death with (solid) and without (dashed) preconditioning. (Right) Repair outcomes under insults of fixed strength but increased durations with (red dots) and without (black boxes) preconditioning (duration = 10 min, 30 days of recovery).

(E) Representative micrographs of Picro Sirius Red staining show collagen deposition in kidney cortex and juxta medulla area in both groups of preconditioned mice and single-IRI mice 30 days after varying degree IRI. Scale bar, 100 μm.

(F–H) Dependence of the level of serum creatinine (F) (n=3), the fraction of the fibrotic area (G), and the animal death fraction (H) on the duration of IRI 30 days after IRI. Preconditioning: 10 min IRI followed by 30 days of recovery.

See also Figure S3.

However, the preconditioned system produced a high level of myofibroblasts (Figure 3A right, red solid line). Thus, the model predicted that ischemic preconditioning increases the risk of CKD. Because the preconditioned state represents iPARS, Wnt, myofibroblasts, and pEMT tubular cells are predicted to persist. This prediction is consistent with clinical observations that some patients, who survive an episode of AKI with no obvious residual impairment of renal function, have significantly increased risk of developing CKD (Chawla and Kimmel, 2012; Coca et al., 2012). Using our computational model, we also tested if repetitive mild AKI, with episodes of different duration and different spacing between episodes, increased the risk of CKD. Our model indicated that some dead tubular cells persisted after each episode and that the level of myofibroblasts increased after each episode (Figures S3A and S3B). Additionally, prolonged and more frequent exposure to mild AKI resulted in quicker development of CKD (Figure S3C). Thus, our simulations recapitulated both the clinical and animal model observations that repetitive mild AKI also increased the risk of CKD (Nath et al., 2000; Thakar et al., 2011).

The previous simulations tested the induction of iPARS on the outcome of a mild second insult (15 min). We also tested the induction of iPARS on the outcome of a stronger second insult (30 min). An insult of this intensity is predicted to sometimes lead to death in the naive control systems (Figures 2C and 2E). Our model predicted that iPARS reduced the peak percentage and cumulative sum of dead tubular cells (Figure 3B, black dashed lines), thus preventing organism death (Figure 3B right, dotted vertical line). This reduction in dead tubular cells was predicted for a large range of durations of the second insult (Figure 3C), indicating that iPARS has a protective role in reducing the risk of death from subsequent severe renal injury.

Taken together, our model predicted that the relative benefit of ischemic preconditioning of kidneys to place them in iPARS depended on the severity of the second insult. When the second insult was severe, the benefit of ischemic preconditioning in reducing the risk of death exceeds that of the increased fibrotic risk associated with MARS, which reflects an increased risk of CKD. Ischemic preconditioning raised the threshold of death and lowered that of MARS (Figure 3D left, blue and green arrows), thus expanding the insult conditions (parameters in the model) associated with survival at the cost of increasing the risk of chronic fibrosis (Figure 3D right).

To test the mathematical predictions, we preconditioned mice by subjecting them to 10-min IRI. After 30 days of recovery, the mice survived and then were exposed to various durations of a second IRI from 10 to 30 min. We observed larger fibrotic patches in both cortex and medulla in all groups of preconditioned mice subjected to a second IRI compared with the animals only subjected to a single IRI (Figure 3E). Serum creatinine levels did not reveal an obvious change in renal function between mice subjected to preconditioning and a second IRI and those subjected to a single IRI (Figure 3F). However, quantification of the fibrotic areas revealed a significant increase of fibrosis in the preconditioned mice compared with the single IRI group (Figure 3G), consistent with the predictions of the model. Also consistent with the model predictions, we observed significant protection from death in the animals subjected to preconditioning, especially for cases of more intense insult (Figure 3H). Thus, these animal experiments recapitulated the opposing effects of preconditioning predicted by the model: Preconditioning reduced death rate at the cost of increased fibrosis.

Wnt-Mediated Positive Feedback Loops Modulate the Repair Response and Risk of Progression to CKD

To explore the molecular origin of the four AKI outcomes, we focused on the positive feedback loop formed by the pEMT tubular cells and Wnt (Figure 2A). We selected this feedback loop because it represents a critical aspect of tissue repair (pEMT tubular cells) and a major contributing factor to fibrosis (Wnt secretion that stimulates myofibroblast expansion). With the model, we tested the effect of altering Wnt signaling on the outcome of injury (Figure 4). From a clinical standpoint, Wnt signaling represents a potentially pharmacologically manipulatable aspect of the injury response; thus, we focus on the results of those simulations.

We simulated the outcomes in the cellular network model by perturbing the activity of Wnt. When we reduced Wnt in the network model, the system tolerated higher insult intensities before jumping to either iPARS or MARS (Figure 4A, blue lines compared with black lines). When we increased Wnt, the system jumped to iPARS and MARS at lower insult intensities (Figure 4A, compare red lines with black lines). These results indicated that reducing Wnt in the presence of a continuous low-intensity insult was protective, increasing the threshold of MARS and making the maladaptive response less likely, whereas increasing Wnt had the opposite effect under these conditions.

We also simulated the outcomes in response to a single transient insult of varying duration representing AKI, while increasing or decreasing Wnt (Figures 4B–4E). When Wnt was reduced, there were only three states: PARS, iPARS, and death. The insult durations that resulted in death or iPARS increased, expanding those states and eliminating MARS (Figures 4B and 4C). Conversely, when Wnt was increased, the insult durations that resulted in MARS increased and fewer resulted in death or iPARS (Figures 4D and 4E), thus raising the threshold for death and lowering that for MARS.

We simulated the effect of Wnt agonists added prior to a single transient insult of varying duration. The model predicted that pretreatment with Wnt agonists raised the threshold of death and expanded the insults that resulted in MARS (Figure 4F). The predicted reduction in death is consistent with a report that treatment with Wnt reduced the kidney damage and improved renal function in an IRI rat model (Kuncewitch et al., 2015). Inspection of the transition between iPARS and MARS (Figure 4F) suggested that the effect of Wnt pathway activity was biphasic: The threshold of MARS first increased (reflecting a safer effect of Wnt treatment) and then decreased as Wnt agonists increased. These results predicted that the therapeutic window for Wnt activation that minimizes both the risk of death from acute injury and the development of chronic fibrosis is narrow.

Consistently, increasing the Wnt secretion rate in the model increased the death threshold and decreased the MARS threshold (Figure 4F). That is, the renal system faces a fundamental trade-off between CKD (represented as MARS) and death, so reducing the risk of death increases the risk of CKD and vice versa. Thus, the model predicted that the consequences of manipulating Wnt consistently throughout the injury response are complicated and depend on the condition (low intensity and continuous injuries, like CKD, or transient injury, like AKI). In CKD, reducing Wnt is predicted to be protective. However, in AKI, reducing Wnt is predicted to increase the risk of death. Furthermore, adding Wnt agonists as a pretreatment strategy is predicted to have a narrow optimal activity window.

Achieving Optimal Treatment of AKI by Dual Targeting of Repair and Resolution Dynamics

In view of the trade-off between repair and fibrosis and the narrow therapeutic window of Wnt activity predicted by our cellular interaction model, we hypothesized that an optimal strategy targeting Wnt would combine activation and inhibition in a temporally controlled manner, thereby promoting both the repair and resolution phases of the injury response. Thus, we formulated it as a computational multi-objective optimization problem and used a Metropolis search to evaluate Wnt-targeted regimens by varying the schedules, durations, and dosages of both Wnt antagonists and agonists (Figure 5A, see Methods). The ideal strategy minimizes both the risks of death and fibrosis and achieves the fastest recovery using the lowest doses of drugs with the shortest treatment time. Practically the optimization process is to minimize a score function that includes all these factors with the highest weight given to reducing the risk of death, followed by the weight for reducing the risk of fibrosis. As expected, the optimal strategy required treatment with a Wnt agonist at the beginning followed by treatment with a Wnt antagonist (Figures 5B and S4A). Simulation of 1,000 mice, each with parameters drawn from a distribution to account for individual

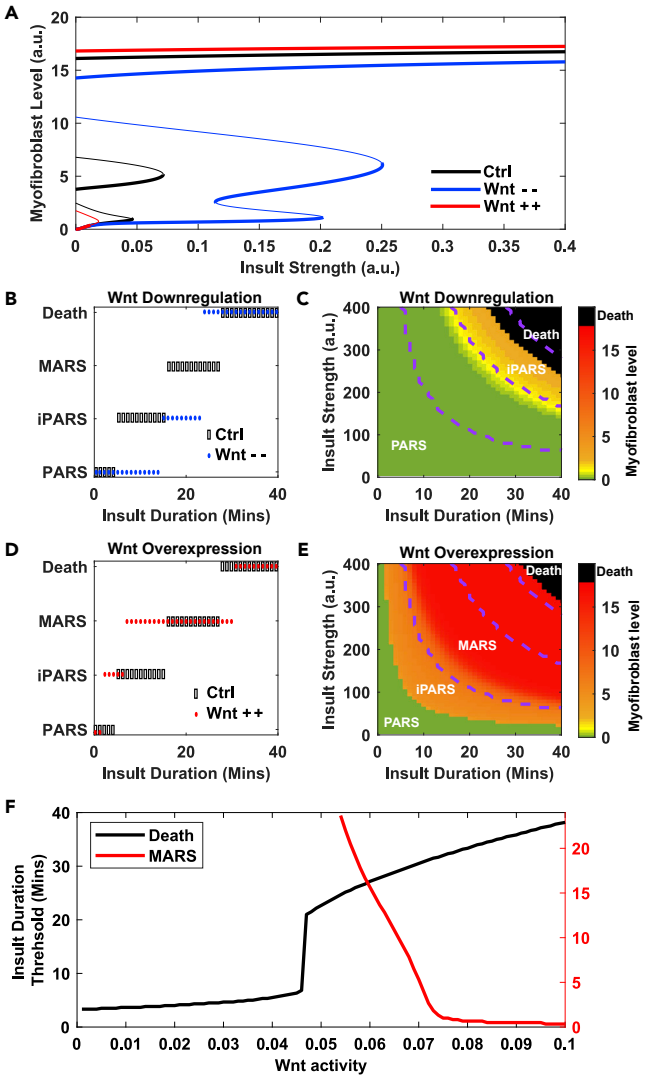

Figure 4. The pEMT-Wnt Axis Modulates Repair Response and Progression Risk to CKD

(A) Bifurcation diagram with overexpressed Wnt (increased secretion rate, red lines) or downregulated Wnt (reduced secretion rate, blue lines) in contrast to the control (Ctrl, black lines).

(B) Repair outcomes under insults of fixed strength but increasing durations with (blue dots) and without (black boxes, control) constant Wnt downregulation.

(C) Phase diagram of repair outcomes (indicated by myofibroblast level) in the space of insult strength and duration with constant downregulated Wnt. Dashed lines indicate boundaries in the control system (without Wnt downregulation).

(D) Repair outcomes under insults of fixed strength but increasing durations of IRI with (red dots) and without (black boxes, control) Wnt constant overexpression.

(E) Same as panel C except with constant Wnt overexpression. Dash lines represent the boundaries in the control system (without Wnt overexpression).

(F) Effect of Wnt agonist treatment before AKI on repair outcome under various insult duration.

heterogeneity confirmed the robustness of the treatment scheme with the most mice under a combined treatment of Wnt agonist and antagonist reaching PARS and a small fraction reaching iPARS (Figure 5C). Our model also predicted that the optimal treatment design depends on insult duration (Figures S4B and S4C).

To validate our therapeutic strategy, we used a 30-min IRI and tested four different treatment designs in mice: IRI only, a single Wnt1 pretreatment prior to IRI, Wnt signal inhibitor ICG-001 treatment administered

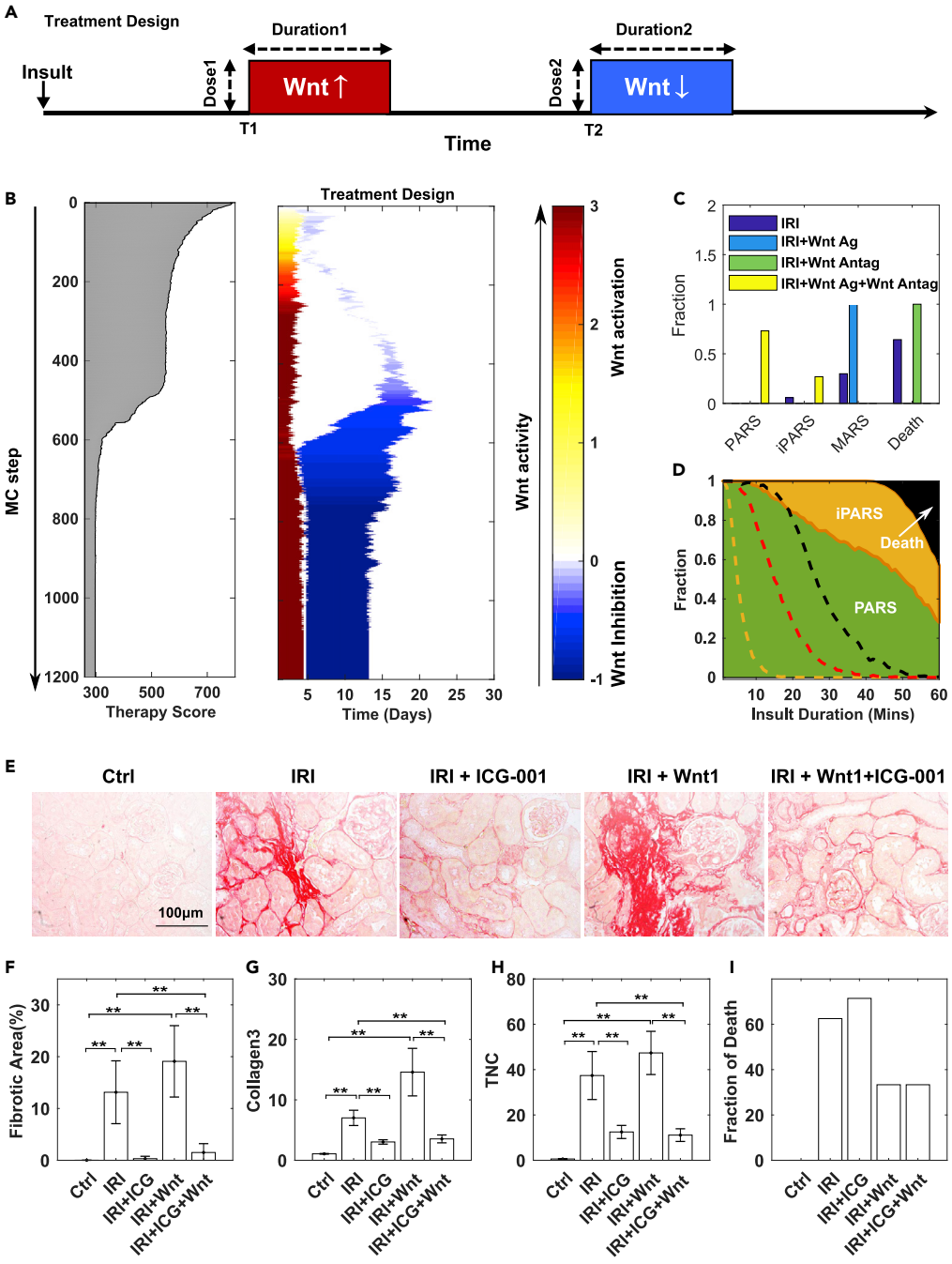

Figure 5. Temporal Regulation of Wnt Represents the Optimal Dynamic Treatment Design for AKI through Temporal Regulation of Wnt

(A)Schematic of treatment design combining Wnt and its inhibitor, with parameters to be optimized including the doses, timings, and durations of Wnt and inhibitor.

(B) Representative searching trajectory of the therapy score function and treatment design over Monte Carlo steps. The weights of different factors [λ1, λ2, λ3, λ4, λ5] in the score function are set as [500, 10, 1, 1, 1].

(C) Fraction of various repair outcomes under different treatment designs—Wnt agonist only (Wnt Ag), Wnt antagonist (Wnt Antag), or combination of Wnt agonist and antagonist—and the control system without treatment, each sampled from 1,000 simulations.

(D) Fractions of repair outcomes as a function of insult duration with the optimal design for the 30-min insult. Dashed lines are corresponding region boundaries without treatment (yellow, PARS/iPARS; red, iPARS/MARS; black, MARS/Death). Each result was sampled from 1,000 independent simulations.

Figure 5. *Continued*

(E–I) Representative micrographs of Picro Sirius Red staining (E), the fraction of fibrotic area (F), quantitative real-time RT-PCR (qRT-PCR) for collagen type III and TNC (G and H) on day 30 and the fraction of animal death (I) (within 30 days) after 30-min IRI with pre-administration of Wnt treatment or with Wnt inhibitor ICG-001 administration from day 4 to day 30 or combination of Wnt pre-administration and ICG-001 administration from day 4 to day 30 or without any treatment. Scale bar, 100 μm. **$p < 0.01$ versus labeled groups using one-way ANOVA, followed by the Student-Newman-Keuls test ($n = 4–6$). For (I), the total number of mice is 9–16 for each group. For (F)–(H), data are represented as mean ± SEM. See also Figures S4–S6 and Table S3.

every day from day 4 to day 13 after IRI, and combined treatment with Wnt1 before IRI and ICG-001 after IRI. Of note, the Wnt1 pretreatment was based on the hydro-dynamic gene delivery technique. Figure S5 illustrated that HA-tagged Wnt1 gene was effectively delivered to the kidneys. Histochemical analysis showed that fibrosis was markedly reduced in the groups receiving ICG-001 alone or in combination with Wnt1 pretreatment; pretreatment with Wnt1 alone increased the severity of fibrosis (Figures 5E and 5F). Compared with the IRI-only group, we observed a reduction of components of the extracellular matrix, indicating reduced extracellular matrix deposition, in the groups with combined treatment or ICG-001-only treatment, whereas Wnt1 pretreatment alone increased extracellular matrix deposition (Figures 5G and 5H). Either Wnt1 pretreatment alone or the combination treatment enhanced survival to this severe insult (Figure 5I). In the absence of ischemic insults, administration of either Wnt1 or ICG-001 alone had little effect (Figure S6), recapitulating our previous findings (Xiao et al., 2016; Zhou et al., 2018).

Taken together, the prediction from theoretical analysis and preclinical studies in a mouse model for AKI and CKD suggested that combined sequential treatment with Wnt agonists and antagonists can overcome the dilemma of the double-edged-sword effect of Wnt pathway activity and minimize both animal death and kidney fibrosis.

DISCUSSION

Tissue injury and its repair pose a conundrum that lies at the intersection between recovery from acute disease and the development of chronic disease. The unleashing of a well-orchestrated and rapid response that fixes the parenchymal tissue defect through a transient mesenchymal proliferative response must be tightly controlled to prevent chronic fibrosis caused by the response itself. Thus, tissue repair that ensures survival ranges from full reconstitution to chronic disease. The latter represents an evolutionary trade-off that prioritizes survival over avoidance of proliferative fibrotic disease.

We used an established animal model for acute ischemic kidney injury in the mouse to study the trade-off using both experimental and mathematical analyses. By multi-variable molecular, morphological, and functional assessment, we identified three distinct response types of kidney tissue with respect to its adaptation to the insult: full recovery of the healthy tissue (PARS), functional recovery with residual tissue alterations (iPARS), and progressive chronic disease with fibrosis (MARS).

It is increasingly believed that the acute and chronic forms of kidney disease do not reflect distinct types of diseases with different etiologies. Instead, both forms are distinct responses to the same type of insult, such as ischemia, occurring at varying intensity. Thus, the system is a dynamical one producing qualitatively distinct behaviors in response to a quantitative continuum of perturbation. The emergence of multiple qualitatively distinct behaviors is a central characteristic of non-linear dynamical systems. Therefore, dynamical systems theory is an appropriate method for analyzing the system representing the kidney injury response.

In constructing a mathematically tractable model, we focused on the repair of the cellular damage mediated by well-characterized cell-to-cell interactions. The dynamics of the cell interaction network (Figure 2A) exhibited multistable dynamics that mapped to the four observed disease fates: PARS, iPARS, MARS, and death. Theoretical analysis of the model made a number of predictions that were experimentally confirmed and explained long-observed phenomena (Figure 6 and Table S3). Multistability and memory are the most elementary manifestations of non-linear dynamics and require positive feedback loops in the system architecture (Angeli et al., 2004). Memory is a manifest of irreversibility, which emerges owing to hysteresis in the dynamics. Physiologically, memory is represented in iPARS as the remnants of tissue pathology that persist long after the end of ischemia and in MARS as the progression to fibrosis. Memory is also represented by the protective priming effect of pre-conditioning, a phenomenon seen in several ischemic organ diseases. Thus, the kidney repair program keeps a "memory" of previous injury and is primed for a more rapid

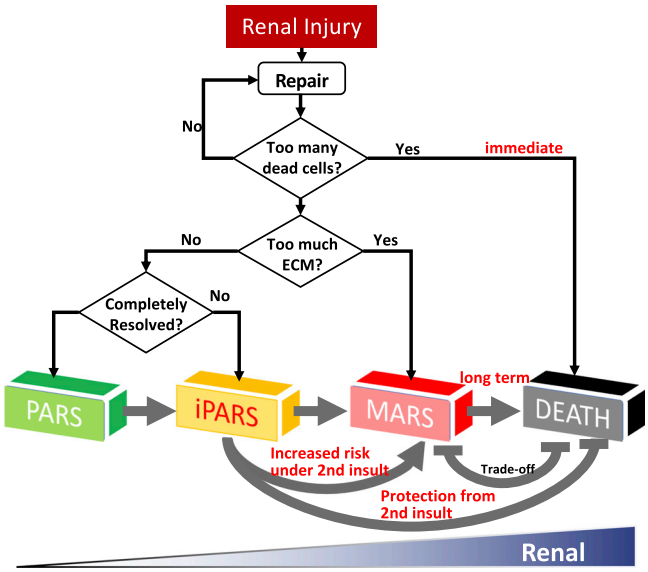

Figure 6. Summary of the Renal Repair Process

In response to injury, the renal repair system is initialized to reduce the damage through cell regeneration. If too many tubular cells are dead without timely replenishment, immediate death may happen. Otherwise, the repair process continues and generates myofibroblast that produces extracellular matrix (ECM). If too much ECM accumulates, the system goes into MARS and develops renal fibrosis. If the ECM level is low and the level of myofibroblasts does not reset to the pre-injury level, the system goes into iPARS. If all the components are completely reset to their normal states, the system goes into PARS. See also Table S4.

response to subsequent injury but at the expense of increased risk of fibrosis. Future studies may further reveal the molecular mechanisms of the memory, including possible roles of epigenetic modifications.

The double-edged nature of molecular players that could serve as therapeutic targets poses a dilemma for treatment. Specifically, Wnt represents an important lever point for pharmacological intervention. However, Wnt plays opposing roles, which are captured in our model: in the acute phase, it is a positive regulator of regeneration by promoting stem-like states and stimulating myofibroblast expansion. However, the latter role of Wnt signaling drives fibrosis in the chronic phase. Some studies indicate renal tubular cells undergoing pEMT are a potential target for intervention as tubular cells in pEMT state secrete various cytokines to promote the fibrosis (Grande et al., 2015; Lovisa et al., 2015), and others focus on the activation of resident fibroblasts as a site for intervention because these cells are a source of the fibrogenic myofibroblasts (Grande et al., 2015; LeBleu et al., 2013; Lovisa et al., 2015; Nieto et al., 2016; Ovadya and Krizhanovsky, 2015). Both mathematical modeling and experimental studies have identified key pEMT regulators, such as Snail1, HIPK2, NF-κB, and Twist1 (Grande et al., 2015; Jin et al., 2012; Lovisa et al., 2015; Tian et al., 2013; Xing and Tian, 2019; Zhang et al., 2014), which may be combined with other targets, such as Wnt and Shh, for designing optimal treatment against both AKI and CKD (Machado and Diehl, 2018; Zhang et al., 2016). However, these approaches commonly rest on the conventional paradigm of linear causation embodied by molecular pathways that only need to be manipulated in one direction (enhanced or inhibited), ideally at multiple points in the network by combination therapy.

However, such unidirectional up- or downregulation of pathways cannot address the complexity of a trade-off response. Because of the double-edged effect, a unidirectional (unimodal) intervention in the repair program is unlikely to achieve speedy repair and complete resolution, free of unintended consequences. Thus, we focused on the double-edged sword effect of Wnt as a potential target, for which both agonists and antagonists exist. We formulated a treatment design as an optimization problem. Our computational optimization procedure proposed a regimen that we implemented in the animal AKI model, demonstrating that a temporal combination of applying a Wnt agonist and a Wnt antagonist thereafter can both prevent death by promoting rapid repair as well as reduce the development of fibrosis. That is, Wnt antagonists could prevent fibrosis. However, Wnt

signaling is necessary to activate regenerative programs. Indeed, in studies with mice, Wnt agonists administered prior to an ischemic episode reduce kidney damage and improve renal function (Kuncewitch et al., 2015). The key to using Wnt pathway-targeted therapies is timing the application of the agonists and antagonists. Agonists need to be administered early after the injury to promote repair, whereas antagonists need to be administered later to enable resolution and limit fibrosis. Future studies with time-controlled, cell-type-specific genetic models are warranted to further address this issue.

While the broader applicability of our procedure of optimizing the dual use of antagonist and agonist to control the non-linear dynamics of the repair process remains to be further evaluated in human and other disease models, our results suggest that, to confront a pathogenetic mechanism that involves a target that is a double-edged sword, we need to think beyond the standard unidirectional inhibition (or activation) of a single target or pathway. As a first step, our work establishes the rationale for a new modality of non-monotonical pharmacological intervention to control non-linear disease dynamics by biphasic application of both agonists and antagonists of the same target. The insights provided by the current work may guide potential therapeutic strategies, which would need rigorous investigation before any practical clinical intervention.

Limitations of the Study

In this work, we presented a proof-of-concept study focusing on Wnt signaling in the context of fibrosis. Our model robustly predicts key dynamic features of the repair response that underlies the pathogenesis. As with any model, some simplification is necessary to enable computational study. Two cell types (tubular epithelial cells and fibroblast cells) and two pathways (Shh and Wnt) are considered in the model, which works despite the simplicity. Thus, our model implicitly but not explicitly takes into account a number of molecular mechanisms known to take part in the response, such as several inflammatory cytokines, growth factors, autacoids, and ECM (Bonventre and Zuk, 2004). By focusing on regeneration that repairs the cellular deficit caused by ischemic destruction, we omit inflammatory infiltrates and ensuing angiogenesis. Through implementing these processes and their actively controlled termination, future studies may fine-tune the model description of disease course with genetic mouse models. In addition, our cell-cell interaction model describes tissue-level changes (as defined by cell and matrix composition) and does not consider the granularity to describe gene expression changes and associated epigenetic alterations that govern the cell state dynamics and have been implicated in the memory of AKI (Naito et al., 2009; Ramesh and Reeves, 2004; Zager and Johnson, 2009). The spatial aspects were not considered in the model. Considering spatial aspects in the mathematic model and targeting the EMT plasticity will further optimize the treatment design (Goetz et al., 2020).

METHODS

All methods can be found in the accompanying Transparent Methods supplemental file.

DATA AND CODE AVAILABILITY

All data produced or analyzed for this study are included in the published article and its supplementary information files or are available from the corresponding author upon reasonable request. All the equations and parameters of the mathematical models can be found in Transparent Methods.

SUPPLEMENTAL INFORMATION

Supplemental Information can be found online at https://doi.org/10.1016/j.isci.2020.101047.

ACKNOWLEDGMENTS

The project was supported by the National Science Foundation through grant DMS-1462049 (to J.X.), EF-1921412 (to X.-J.T); the National Institutes of Health through Grant DK119232 (to J.X.), DK064005 (to Y.L.), DK106049 (to Y.L.), DK116816 (to D.Z.), UL1TR001857 (to the University of Pittsburgh); the National Science Foundation of China (NSFC) grant 81521003 (to Y.L.); and Guangdong Science Foundation Innovative Group Grant 2014A030312014 (to Y.L.). H.F. was supported by NSFC grants 81770737 and 81970587. We thank Nancy R. Gough (BioSerendipity, LLC) for critical discussions and editorial assistance.

AUTHOR CONTRIBUTIONS

Conceptualization, X.-J.T., D.Z., Y.L., and J.X.; Methodology, X.-J.T., D.Z., H.F., R.Z., and X.W.; Investigation, X.-J.T., D.Z., H.F., R.Z., X.W., Y.L., and J.X.; Writing – Original Draft, X.-J.T., D.Z., and J.X.; Writing – Review

& Editing, X.-J.T., D.Z., Y.L., J.X., and S.H.; Funding Acquisition, Y.L., J.X., X.-J.T., and D.Z.; Resources, Y.L. and J.X.; Supervision, Y.L. and J.X.

DECLARATION OF INTERESTS

The authors declare no conflict of interest.

Received: October 2, 2019
Revised: March 15, 2020
Accepted: April 5, 2020
Published: May 22, 2020

REFERENCES

Akhmetshina, A., Palumbo, K., Dees, C., Bergmann, C., Venalis, P., Zerr, P., Horn, A., Kireva, T., Beyer, C., Zwerina, J., et al. (2012). Activation of canonical Wnt signalling is required for TGF-β-mediated fibrosis. Nat. Commun. *3*, 735.

Amdur, R.L., Chawla, L.S., Amodeo, S., Kimmel, P.L., and Palant, C.E. (2009). Outcomes following diagnosis of acute renal failure in U.S. veterans: focus on acute tubular necrosis. Kidney Int. *76*, 1089–1097.

Angeli, D., Ferrell, J.E., Jr., and Sontag, E.D. (2004). Detection of multistability, bifurcations, and hysteresis in a large class of biological positive-feedback systems. Proc. Natl. Acad. Sci. U S A *101*, 1822–1827.

Belayev, L.Y., and Palevsky, P.M. (2014). The link between acute kidney injury and chronic kidney disease. Curr. Opin. Nephrol. Hypertens. *23*, 149–154.

Bonventre, J.V. (2002). Kidney ischemic preconditioning. Curr. Opin. Nephrol. Hypertens. *11*, 43–48.

Bonventre, J.V., and Zuk, A. (2004). Ischemic acute renal failure: an inflammatory disease? Kidney Int. *66*, 480–485.

Chawla, L.S., and Kimmel, P.L. (2012). Acute kidney injury and chronic kidney disease: an integrated clinical syndrome. Kidney Int. *82*, 516–524.

Coca, S.G., Yusuf, B., Shlipak, M.G., Garg, A.X., and Parikh, C.R. (2009). Long-term risk of mortality and other adverse outcomes after acute kidney injury: a systematic review and meta-analysis. Am. J. Kidney Dis. *53*, 961–973.

Coca, S.G., Singanamala, S., and Parikh, C.R. (2012). Chronic kidney disease after acute kidney injury: a systematic review and meta-analysis. Kidney Int. *81*, 442–448.

Ferenbach, D.A., and Bonventre, J.V. (2015). Mechanisms of maladaptive repair after AKI leading to accelerated kidney ageing and CKD. Nat. Rev. Nephrol. *11*, 264–276.

Gardet, A., Zheng, T.S., and Viney, J.L. (2013). Genetic architecture of human fibrotic diseases: disease risk and disease progression. Front. Pharmacol. *4*, 159.

Goetz, H., Melendez-Alvarez, J.R., Chen, L., and Tian, X.J. (2020). A plausible accelerating function of intermediate states in cancer metastasis. PLoS Comput. Biol. *16*, e1007682.

Grande, M.T., Sanchez-Laorden, B., Lopez-Blau, C., De Frutos, C.A., Boutet, A., Arevalo, M., Rowe, R.G., Weiss, S.J., Lopez-Novoa, J.M., and Nieto, M.A. (2015). Snail1-induced partial epithelial-to-mesenchymal transition drives renal fibrosis in mice and can be targeted to reverse established disease. Nat. Med. *21*, 989–997.

Grgic, I., Duffield, J.S., and Humphreys, B.D. (2012). The origin of interstitial myofibroblasts in chronic kidney disease. Pediatr. Nephrol. *27*, 183–193.

Humphreys, B.D. (2018). Mechanisms of renal fibrosis. Annu. Rev. Physiol. *80*, 309–326.

Jin, Y., Ratnam, K., Chuang, P.Y., Fan, Y., Zhong, Y., Dai, Y., Mazloom, A.R., Chen, E.Y., D'Agati, V., Xiong, H., et al. (2012). A systems approach identifies HIPK2 as a key regulator of kidney fibrosis. Nat. Med. *18*, 580–588.

Joo, J.D., Kim, M., D'Agati, V.D., and Lee, H.T. (2006). Ischemic preconditioning provides both acute and delayed protection against renal ischemia and reperfusion injury in mice. J. Am. Soc. Nephrol. *17*, 3115–3123.

Koh, T.J., and DiPietro, L.A. (2011). Inflammation and wound healing: the role of the macrophage. Expert Rev. Mol. Med. *13*, e23.

Kuncewitch, M., Yang, W.L., Corbo, L., Khader, A., Nicastro, J., Coppa, G.F., and Wang, P. (2015). WNT agonist decreases tissue damage and improves renal function after ischemia-reperfusion. Shock *43*, 268–275.

Kusaba, T., Lalli, M., Kramann, R., Kobayashi, A., and Humphreys, B.D. (2014). Differentiated kidney epithelial cells repair injured proximal tubule. Proc. Natl. Acad. Sci. U S A *111*, 1527–1532.

LeBleu, V.S., Taduri, G., O'Connell, J., Teng, Y., Cooke, V.G., Woda, C., Sugimoto, H., and Kalluri, R. (2013). Origin and function of myofibroblasts in kidney fibrosis. Nat. Med. *19*, 1047–1053.

Leung, K.C.W., Tonelli, M., and James, M.T. (2013). Chronic kidney disease following acute kidney injury[mdash]risk and outcomes. Nat. Rev. Nephrol. *9*, 77–85.

Li, B., Lang, X., Cao, L., Wang, Y., Lu, Y., Feng, S., Yang, Y., Chen, J., and Jiang, H. (2017). Effect of remote ischemic preconditioning on postoperative acute kidney injury among patients undergoing cardiac and vascular interventions: a meta-analysis. J. Nephrol. *30*, 19–33.

Lovisa, S., LeBleu, V.S., Tampe, B., Sugimoto, H., Vadnagara, K., Carstens, J.L., Wu, C.C., Hagos, Y., Burckhardt, B.C., Pentcheva-Hoang, T., et al. (2015). Epithelial-to-mesenchymal transition induces cell cycle arrest and parenchymal damage in renal fibrosis. Nat. Med. *21*, 998–1009.

Lyons, J.P., Mueller, U.W., Ji, H., Everett, C., Fang, X., Hsieh, J.C., Barth, A.M., and McCrea, P.D. (2004). Wnt-4 activates the canonical beta-catenin-mediated Wnt pathway and binds Frizzled-6 CRD: functional implications of Wnt/beta-catenin activity in kidney epithelial cells. Exp. Cell Res. *298*, 369–387.

Machado, M.V., and Diehl, A.M. (2018). Hedgehog signalling in liver pathophysiology. J. Hepatol. *68*, 550–562.

Naito, M., Zager, R.A., and Bomsztyk, K. (2009). BRG1 increases transcription of proinflammatory genes in renal ischemia. J. Am. Soc. Nephrol. *20*, 1787–1796.

Nath, K.A., Croatt, A.J., Haggard, J.J., and Grande, J.P. (2000). Renal response to repetitive exposure to heme proteins: chronic injury induced by an acute insult. Kidney Int. *57*, 2423–2433.

Nieto, M.A., Huang, R.Y., Jackson, R.A., and Thiery, J.P. (2016). Emt: 2016. Cell *166*, 21–45.

O'Neal, J.B., Shaw, A.D., and Billings, F.T. (2016). Acute kidney injury following cardiac surgery: current understanding and future directions. Crit. Care *20*, 187.

Ovadya, Y., and Krizhanovsky, V. (2015). A new Twist in kidney fibrosis. Nat. Med. *21*, 975–977.

Park, K.M., Chen, A., and Bonventre, J.V. (2001). Prevention of kidney ischemia/reperfusion-induced functional injury and JNK, p38, and MAPK kinase activation by remote ischemic pretreatment. J. Biol. Chem. *276*, 11870–11876.

Ramesh, G., and Reeves, W.B. (2004). Inflammatory cytokines in acute renal failure. Kidney Int. *66*, S56–S61.

Serhan, C.N., Brain, S.D., Buckley, C.D., Gilroy, D.W., Haslett, C., O'Neill, L.A., Perretti, M., Rossi, A.G., and Wallace, J.L. (2007). Resolution of inflammation: state of the art, definitions and terms. FASEB J. *21*, 325–332.

Tennakoon, A., Izawa, T., Kuwamura, M., and Yamate, J. (2016). Pathogenesis of type 2 epithelial to mesenchymal transition (EMT) in renal and hepatic fibrosis. J. Clin. Med. *5*, 4.

Thakar, C.V., Christianson, A., Himmelfarb, J., and Leonard, A.C. (2011). Acute kidney injury episodes and chronic kidney disease risk in diabetes mellitus. Clin. J. Am. Soc. Nephrol. *6*, 2567–2572.

Tian, X.J., Zhang, H., and Xing, J. (2013). Coupled reversible and irreversible bistable switches underlying TGFβ-induced epithelial to mesenchymal transition. Biophys. J. *105*, 1079–1089.

Wang, Y., Zhou, C.J., and Liu, Y. (2018). Wnt signaling in kidney development and disease. Prog. Mol. Biol. Transl. Sci. *153*, 181–207.

Willis, B.C., Liebler, J.M., Luby-Phelps, K., Nicholson, A.G., Crandall, E.D., du Bois, R.M., and Borok, Z. (2005). Induction of epithelial-mesenchymal transition in alveolar epithelial cells by transforming growth factor-beta1: potential role in idiopathic pulmonary fibrosis. Am. J. Pathol. *166*, 1321–1332.

Wynn, T.A. (2008). Cellular and molecular mechanisms of fibrosis. J. Pathol. *214*, 199–210.

Wynn, T.A., and Ramalingam, T.R. (2012). Mechanisms of fibrosis: therapeutic translation for fibrotic disease. Nat. Med. *18*, 1028–1040.

Xiao, L., Zhou, D., Tan, R.J., Fu, H., Zhou, L., Hou, F.F., and Liu, Y. (2016). Sustained activation of Wnt/beta-catenin signaling drives AKI to CKD progression. J. Am. Soc. Nephrol. *27*, 1727–1740.

Xing, J., and Tian, X.J. (2019). Investigating epithelial-to-mesenchymal transition with integrated computational and experimental approaches. Phys. Biol. *16*, 031001.

Yang, L., Besschetnova, T.Y., Brooks, C.R., Shah, J.V., and Bonventre, J.V. (2010). Epithelial cell cycle arrest in G2/M mediates kidney fibrosis after injury. Nat. Med. *16*, 535–543.

Zager, R.A., and Johnson, A.C. (2009). Renal ischemia-reperfusion injury upregulates histone-modifying enzyme systems and alters histone expression at proinflammatory/profibrotic genes. Am. J. Physiol. Renal Physiol. *296*, F1032–F1041.

Zarbock, A., Schmidt, C., Van Aken, H., Wempe, C., Martens, S., Zahn, P.K., Wolf, B., Goebel, U., Schwer, C.I., Rosenberger, P., et al. (2015). Effect of remote ischemic preconditioning on kidney injury among high-risk patients undergoing cardiac surgery: a randomized clinical trial. JAMA *313*, 2133–2141.

Zhang, J., Tian, X.J., Zhang, H., Teng, Y., Li, R., Bai, F., Elankumaran, S., and Xing, J. (2014). TGF-beta-induced epithelial-to-mesenchymal transition proceeds through stepwise activation of multiple feedback loops. Sci. Signal. *7*, ra91.

Zhang, J., Tian, X.J., and Xing, J. (2016). Signal transduction pathways of EMT induced by TGF-β, SHH, and WNT and their crosstalks. J. Clin. Med. *5*, 41.

Zhou, D., Li, Y., Zhou, L., Tan, R.J., Xiao, L., Liang, M., Hou, F.F., and Liu, Y. (2014). Sonic hedgehog is a novel tubule-derived growth factor for interstitial fibroblasts after kidney injury. J. Am. Soc. Nephrol. *25*, 2187–2200.

Zhou, D., Tan, R.J., Fu, H., and Liu, Y. (2016). Wnt/β-catenin signaling in kidney injury and repair: a double-edged sword. Lab. Invest. *96*, 156–167.

Zhou, D., Fu, H., Xiao, L., Mo, H., Zhuo, H., Tian, X., Lin, L., Xing, J., and Liu, Y. (2018). Fibroblast-specific β-catenin signaling dictates the outcome of AKI. J. Am. Soc. Nephrol. *29*, 1257–1271.

iScience, Volume *23*

Supplemental Information

Sequential Wnt Agonist Then Antagonist Treatment Accelerates Tissue Repair and Minimizes Fibrosis

Xiao-Jun Tian, Dong Zhou, Haiyan Fu, Rong Zhang, Xiaojie Wang, Sui Huang, Youhua Liu, and Jianhua Xing

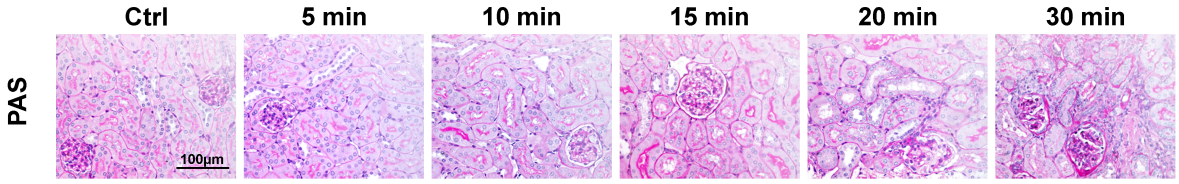

Fig S1. Representative micrographs showing periodic acid-Schiff (PAS) staining in control and diseased kidneys 30 days after varying degrees of IRI. Related to Figure 1. Scale bar, 100 μm.

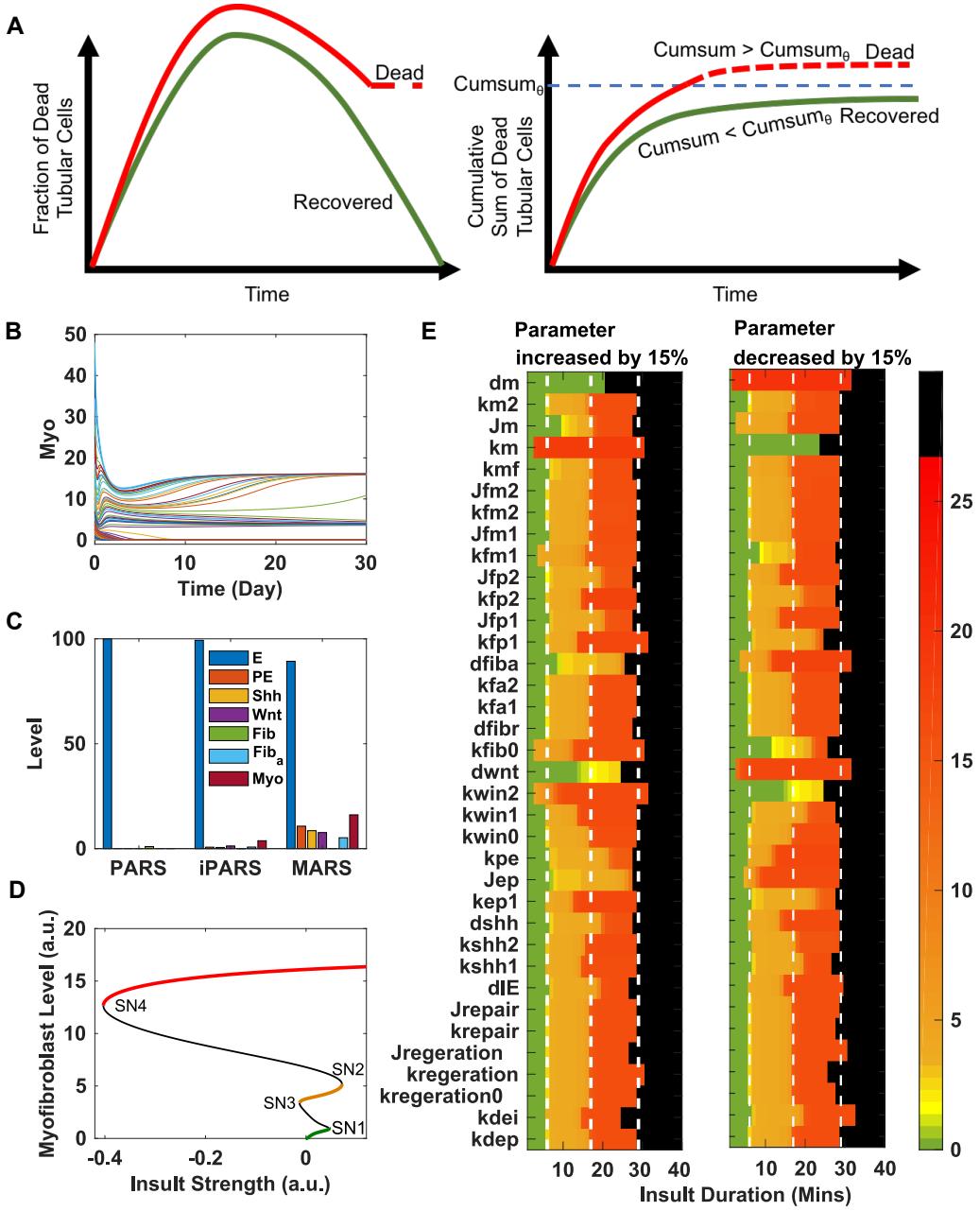

Fig S2. Mathematical definition of the end states. Related to Figure 2.
(A) Definition of death for mathematical simulation. An organism is set to death if the cumulative sum of dead tubular cell ($\int_{t=0}^{t=30day} Odt$) is larger than a threshold ($Cumsum_\theta$).
(B) The simulated time course of the number of myofibroblasts with the system starting from a range of initial conditions
(C) Definition of the states (PARS, iPARS, MARS) in terms of the state variables.
(D) Full bifurcation diagram of the myofibroblast level in respect to insult strength. SN1 and SN2 (SN3 and SN4) indicate the thresholds and irreversibility of iPARS (MARS).
(E) Parameter sensitivity of the thresholds for four outcomes with 15% increase or decrease of each parameter.

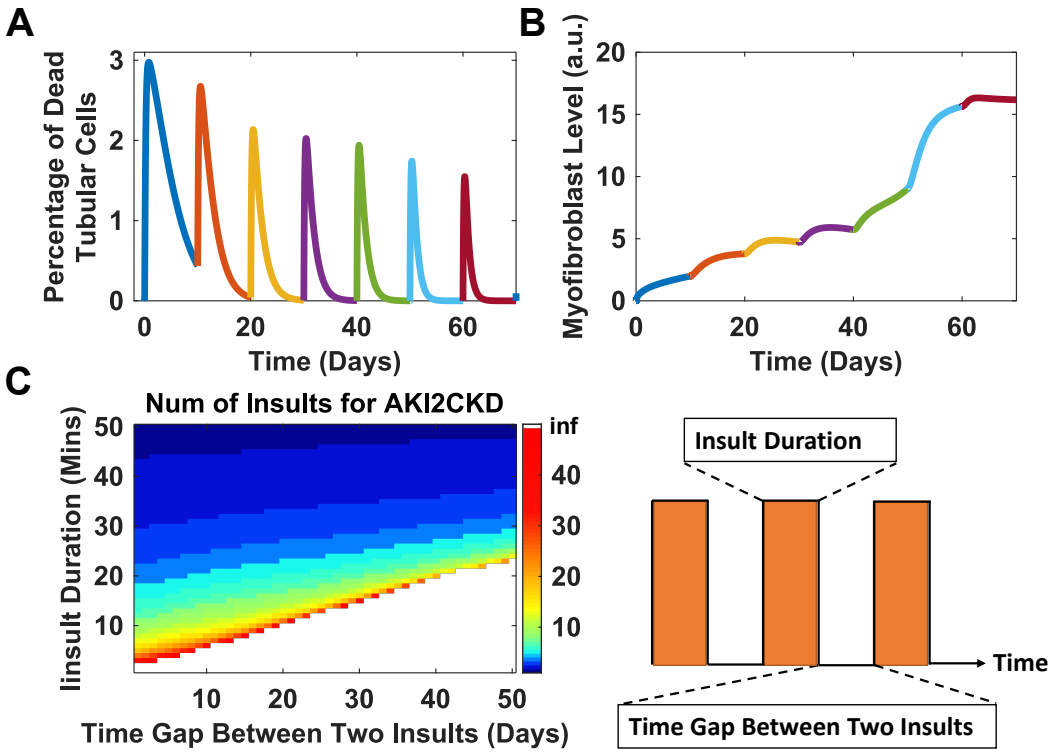

Fig S3. Repeated mild AKI leads to CKD. Related to Figure 3.
(A-B) Temporal profiles of the percentage of dead tubular cells (A) and myofibroblasts (B) under repeated insults (5 min insult every 10 days).
(C) Number of repeated insults needed to induce CKD in the space of insults duration and the gap between two repeated insults.

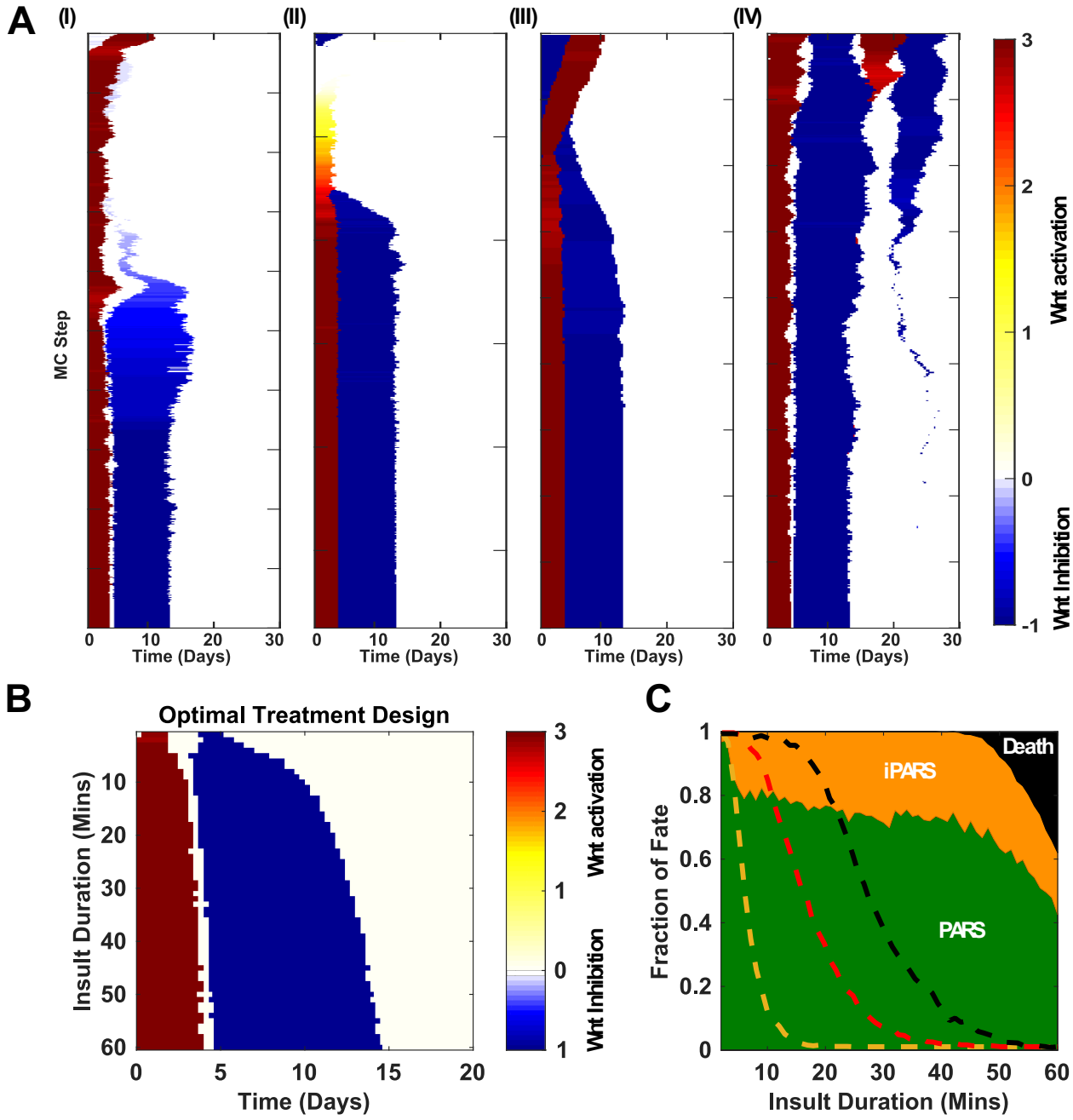

Fig S4. The searching of the optimal treatment design on the starting point and the insult duration. Related to Figure 5.

(A) Representative searching trajectory of the therapy score function and treatment design with a starting point from the initial point with only Wnt mimic at the later phase (I), or an initial point with only Wnt inhibitor at the early phase (II), or an initial point with Wnt inhibitor at the early phase and Wnt mimic after Wnt inhibitor (III), or an initial point with two doses of each drug (IV). (B-C) Fine tuning of the optimal designs according to the insult duration. (B) Optimal design as a function of insult duration. (C) Fractions of repair outcomes as a function of insult duration with duration-specific optimal designs, each sampled with 1000 independent simulations.

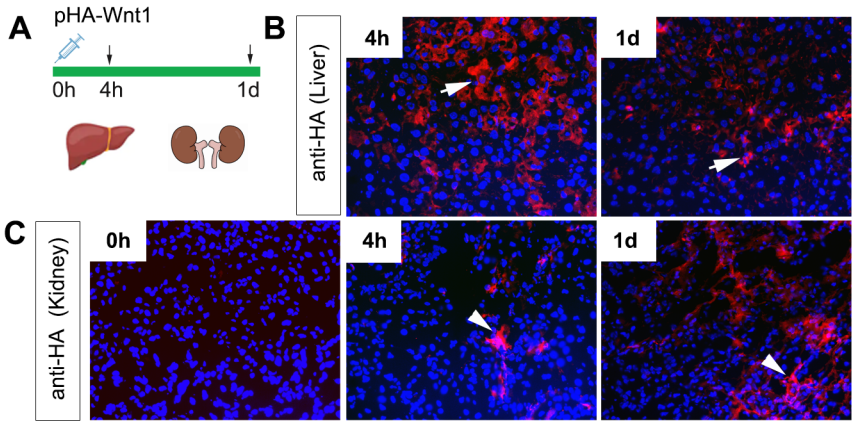

Fig. S5. HA-tagged Wnt1 expression and localization in the liver and kidney after hydrodynamic gene delivery. Related to Figure 5. (A) Schematic diagram. Healthy adult mice were administrated with pHA-Wnt1 intravenously. Liver and kidney tissue were collected at 0h, 4h, and 1d, respectively. (B) HA-tagged Wnt1 in the liver at 4h and 1d after gene delivery. Arrows indicate positive cells. (C) HA-tagged Wnt1 in liver at 4h and 1d after gene delivery. Arrowheads indicate positive cells.

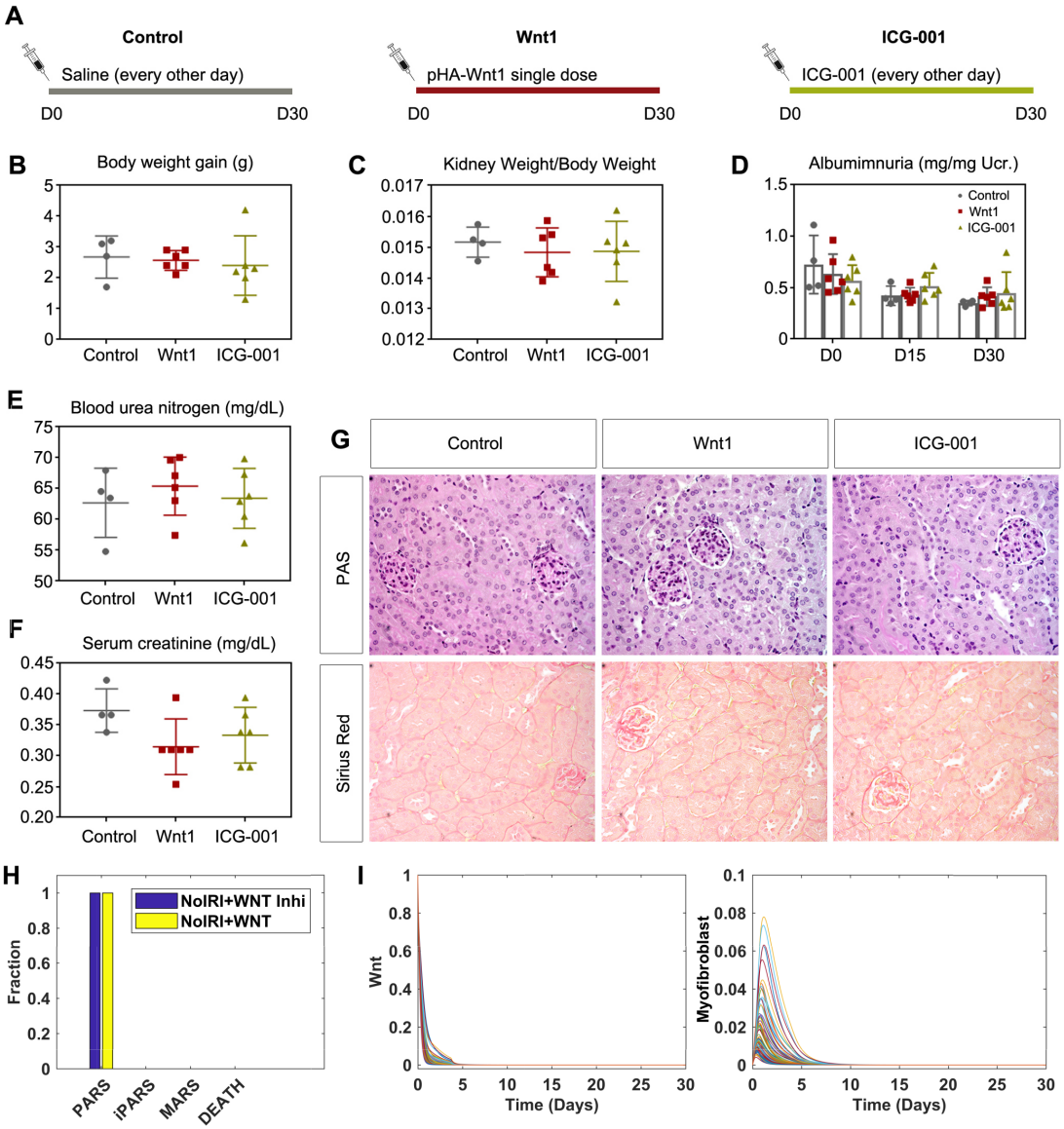

Fig S6. Effect of Wnt or ICG-001 administration in the absence of ischemic insults. Related to Figure 5. (A) Experiment design. (B) Mouse body weight gain at 30 days after Wnt1 or ICG-001 administration, compared with controls (n = 4 - 6). (C) The ratio changes of kidney weight/body weight at 30 days after Wnt1 or ICG-001 administration, compared with controls (n = 4 - 6). (D) Urinary albumin level changes at 30 days after Wnt1 or ICG-001 administration, compared with controls (n = 4 - 6). (E-F) Renal function including blood urea nitrogen (E) and serum creatinine (F) changes at 30 days after Wnt1 or ICG-001 administration, compared with controls (n = 4 - 6). (G) Representative micrographs of PAS or Sirius Red staining show kidney histologic changes or collagen accumulation at 30 days after Wnt1 or ICG-001 administration, compared with controls (n = 3 - 4). (H) Mathematical model behavior in response to Wnt or its inhibitor in the absence of an ischemic insult. (I) Representative simulation results of Wnt and myofibroblast in response to Wnt at absence of an ischemic insult.

Table S1. Parameters of the model. See also the 'Parameter Estimation and Justification'.

Related to Figure 2.

Parameter	Description	Value
kd_{ei}	Rate of tubular cell injury induced by insults	0.001
$k_{regeration0}$	Basic regeneration rate of healthy tubular cells	0.00001
$k_{regeration}$	Regeneration rate of healthy tubular cells mediated by Wnt	0.001
$J_{regeration}$	Michaelis constant of Wnt-dependent regeneration of healthy	5
k_{ep1}	Transition rate from healthy tubular cells to partial EMT tubular	0.11
J_{ep}	Michaelis constant of Wnt-dependent partial EMT	7
k_{pe}	Transition rate from partial EMT tubular cells to healthy tubular	0.5
k_{repair}	Repair rate of injured tubular cells	0.05
J_{repair}	Michaelis constant of Wnt-dependent repair of damaged tubular	0.1
d_{IE}	Death rate of injured tubular cells	0.2
k_{Shh1}	Shh secretion rate from injured tubular cells	0.2
k_{Shh2}	Shh secretion rate from partial EMT tubular cells	0.008
d_{Shh}	Degradation rate of Shh	0.01
k_{win1}	Wnt secretion rate from partial EMT tubular cells	0.06
k_{win2}	Wnt secretion rate from myofibroblasts	0.06
d_{wnt}	Degradation rate of Wnt	0.21
k_{fib0}	Basic production rate of resident fibroblasts	0.1
d_{fibr}	Basic death rate of resident fibroblasts	0.1
k_{fa1}	Activation rate of fibroblasts by Shh	5
k_{fa2}	Activation rate of fibroblasts by Wnt	5
d_{fiba}	Basic death rate of activated fibroblasts	0.1
k_{fp1}	Shh-dependent production rate of fibroblasts	0.15
J_{fp1}	Michaelis constant of Shh-dependent production of fibroblasts	4
k_{fp2}	Wnt-dependent production rate of fibroblasts	0.2
J_{fp2}	Michaelis constant of Wnt-dependent production of fibroblasts	4
k_{fm1}	Transition rate from Shh-dependent fibroblast to myofibroblast	0.1
J_{fm1}	Michaelis constant of Shh-dependent fibroblast to myofibroblast	0.1
k_{fm2}	Transition rate from Wnt-dependent fibroblast to myofibroblast	0.05
J_{fm2}	Michaelis constant of Wnt-dependent fibroblast to myofibroblast	6
k_{mf}	Transition rate from myofibroblast to fibroblast	0.01
k_{m}	Production rate of myofibroblasts	0.1
J_{m}	Michaelis constant of Wnt-dependent production of myofibroblast	0.25
M_{max}	Maximal level of myofibroblasts	60
k_{m2}	Production rate of myofibroblast promoted by partial EMT tubular	0.005
d_{m}	Death rate of myofibroblast	0.1

Table S2. Variables of the model. Related to Figure 2.

Variable	Description	Initial values
E	Percentage of tubular cells in health state	100
IE	Percentage of tubular cells in injured state	0
PE	Percentage of tubular cells in partial EMT state	0
O	Percentage of tubular cells in dead/vacancy state	0
Shh	Level of Shh secreted by tubular cells	0
Wnt	Level of Wnt secreted by tubular cells and myofibroblasts	0
Fib_r	Relative level of resident fibroblasts	1
Fib_a	Relative level of activated fibroblasts	0
Myo	Relative level of myofibroblasts	0

Table S3. Nucleotide sequences of the primers used for RT-PCR. Related to Figure 5.

Mouse gene	Primer Sequence 5' to 3'	
	Forward	**Reverse**
Collagen I	ATCTCCTGGTGCTGATGGAC	ACCTTGTTTGCCAGGTTCAC
Collagen III	AGGCAACAGTGGTTCTCCTG	GACCTCGTGCTCCAGTTAGC
TNC	CAGGAATCTCCGCCGTGTCT	GTGGCTTGCTGGCTCTTTGG
β-actin	CAGCTGAGAGGGAAATCGTG	CGTTGCCAATAGTGATGACC

Table S4. Predictions and experimental confirmations. Related to Figure 6.

The risk of developing progressive CKD is significantly increased even if one patient has survived an episode of AKI	(Belayev and Palevsky, 2014; Leung et al., 2013)
The long-term outcome of AKI varies among patients.	(Belayev and Palevsky, 2014)
Administration of Wnt agonist at one hour prior to ischemia reduces kidney damage and improves renal function	(Kuncewitch et al., 2015)
Ischemic preconditioning provides both acute and delayed protection against renal damage in mice	(Bonventre, 2002; Joo et al., 2006; Park et al., 2003; Park et al., 2001)
Acute kidney injury can be significantly reduced with remote ischemic preconditioning	(Li et al., 2017; Zarbock et al., 2015)
Inhibiting partial EMT reduces fibrosis	(Grande et al., 2015; Lovisa et al., 2015)
Imperfect adaptive response state reduces the risk of death but increases the risk of fibrosis	Predicted and verified here
A dynamic therapy strategy targeting on Wnt is able to reduce the risk of both death and fibrosis.	Predicted and verified here

Transparent Methods

Ethics statement

All animal experiments were conducted using mice bred at and maintained in our animal facility according to the guidelines of the Institutional Animal Care and Use Committee of University of Pittsburgh (19034849 & 19044959).

Animal models

Male BALB/c mice weighing about 22–25 g were obtained from the Envigo (Somerset, NJ). Renal IRI was performed in mice by using an established protocol, as described elsewhere (Zhou et al., 2012). Briefly, bilateral renal pedicles were clamped for designed timing using microaneurysm clamps to generate acute injury. During the ischemic period, body temperature was maintained at 37°C by using a temperature-controlled heating system. Animals were then administered intraperitoneally with buprenorphine at 0.05 mg/kg body wt. For Wnt pretreatment, the mice were subjected to a single intravenous injection of Wnt1 expression plasmid (pHA-Wnt1; Upstate Biotechnology) at 1 mg/kg body wt using the hydrodynamic–based gene transfer technique (Dai et al., 2002; Xiao et al., 2016). Specifically, 20 μg plasmid DNA was diluted in 1.8 ml saline and injected through the tail vein into mouse circulation within 5–10 seconds. Mice from the control group were injected with 20 μg empty vector pcDNA3 in an identical manner. For pharmacologic inhibition experiments, mice were daily intraperitoneal injection of ICG-001-phosphate (kindly provided by Dr. M. Kahn, University of Southern California, Los Angeles, CA) at 5 mg/kg body weight from the 4^{th} day after IRI (Hao et al., 2011; Xiao et al., 2019; Xiao et al., 2016; Zhou et al., 2015). Mice were sacrificed at 30th day after IRI, and serum and kidney tissues were collected for various analyses. Animal experiments were approved by the Institutional Animal Care and Use Committee at the University of Pittsburgh.

Determination of Serum Creatinine

Serum was collected from mice at different times after IRI as indicated. Serum creatinine level was determined by use of a QuantiChrom creatinine assay kit, according to the protocols specified by the manufacturer (BioAssay Systems, Hayward, CA). The level of serum creatinine was expressed as milligrams per 100 ml (dl).

Reverse transcriptase (RT) and real-time PCR

Total RNA isolation and quantitative, real-time RT-PCR (qRT-PCR) were carried out by the procedures (Zhou et al., 2014). Specifically, Total RNA isolation was carried out using the TRIzol RNA Isolation System (Life Technologies, Grand Island, NY) according to the manufacturer's instruction. The first strand cDNA synthesis was carried out by using a Reverse Transcription System kit according to the instructions of the manufacturer (Promega, Madison, WI). qRT-PCR was performed on ABI PRISM 7000 Sequence Detection System (Applied Biosystems, Foster City, CA). The PCR reaction mixture in a 25-μl volume contained 12.5 μl 2x SYBR Green PCR Master Mix (Applied Biosystems), 5 μl diluted RT product (1:10) and 0.5 μM sense and antisense primer sets. PCR reaction was run by using standard conditions. After sequential incubations at 50°C for 2 min and 95°C for 10 min, respectively, the amplification protocol consisted of 40 cycles of denaturing at 95° C for 15 sec, annealing and extension at 60 ° C for 60 sec. The standard curve was made from series dilutions of template cDNA. The mRNA levels of various genes were calculated after normalizing with β-actin. Primer sequences used for amplifications were presented in Table S4.

Histology and immunohistochemical staining

Paraffin-embedded mouse kidney sections (3-μm thickness) were prepared by a routine procedure. The sections were stained with Periodic acid–Schiff (PAS) staining reagents by standard protocol. Immunohistochemical staining was performed according to the established protocol (Zhou et al., 2013a). Specifically, Paraffin-embedded mouse kidney sections (3-μm thickness) were prepared by a routine procedure. The sections were stained with Periodic acid–

Schiff (PAS) staining reagents by standard protocol. For immunohistochemical staining, paraffin-embedded sections were stained with anti-Wnt1 (ab15251); anti-α-SMA (ab5694) (Abcam, Cambridge, MA), anti-FSP-1 (#07-2274; EMD Millipore, Burlington, MA), anti-Vimentin (#5741); and anti-PDGFR-β (#3169) (Cell Signaling Technology, Danvers, MA) antibodies using the routine procedure. Nonimmune normal control IgG was used to replace the primary antibody as negative control, and no staining occurred. Briefly, slides were deparaffinized, with inactivation of endogenous peroxidases and blocking, followed by incubation with primary antibody overnight. Subsequent incubation with biotinylated secondary antibody (Jackson ImmunoResearch Laboratories), ABC Reagent, and AEC Reagent (Vector Laboratories, Burlingame, CA) were used to visualize staining. The antibodies against Wnt1 (ab15251); α-SMA (ab5694) (Abcam, Cambridge, MA), FSP-1 (#07-2274; EMD Millipore, Burlington, MA), Vimentin (#5741); PDGFR-β (#3169) (Cell Signaling Technology, Danvers, MA) were used.

Statistical analyses

All data were expressed as mean ± SEM. Statistical analysis of the data was performed using SigmaStat software (Jandel Scientific Software, San Rafael, CA). Comparison between groups was made using one-way ANOVA, followed by the Student-Newman-Keuls test. $P < 0.05$ was considered significant.

Mathematical modeling and computer simulation for renal homeostasis and fibrosis

In response to renal insults, a complex interconnected wound-healing program is activated to repair the damage. Here we built a minimal mathematical model that explicitly considers the communication of a tubular module and a fibroblast module, while other modules are either implicitly considered or can be added straightforwardly in the future.

After treating a mouse with IRI, some of the tubular cells are injured, which either can be repaired to normal tubular epithelial cells or become dead through apoptosis or necrosis. In addition, tubular cells can be settled in a partial EMT state, which is confined to their tissue of origin, under G2/M cell cycle arrest, and apoptosis resistant (Grande et al., 2015). Thus, we divide tubular cells into three groups, normal tubular epithelial cells (E), injured tubular cells (IE), and partial EMT tubular cells (PE). The fibroblast module includes three groups, resident

fibroblasts, activated fibroblasts and myofibroblasts. At the rest state, a low level of local resident fibroblast cells is kept in inactive state. In response to renal damage, fibroblasts are activated and recruited to the damage sites, and then are transitioned to myofibroblast. Myofibroblast plays a critical role in the repair/regeneration of tubular cells and formation of fibrosis.

One way of communication between the two modules is through secreted growth factors. For example, injured tubular epithelial cells secret Shh to promote activation of local resident fibroblasts and proliferation of myofibroblast (Zhou et al., 2014), while both myofibroblasts and PEs secret Wnt to promote proliferation of normal tubular epithelial cells, repair of the injured tubular cells, and transition from healthy tubular cells into PEs (Zhou et al., 2016). Furthermore, these secreted growth factors do not work alone but in a concerted way. For example, experimental data suggests that HGF and Wnt work inter-dependently to promote proliferation of tubular epithelial cells (Nelson and Nusse, 2004), and Wnt is necessary for TGF-β-mediated myofibroblast activation (Akhmetshina et al., 2012; Maarouf et al., 2016). Thus, here we only consider Wnt and Shh in the model for simplicity. Involvement of other growth factors is implicitly included in the present model, and can be treated explicitly by generalizing the model in the future. Several positive feedback loops exist in the cell-cell communication. For example, PEs secret Wnt while Wnt promotes the transition of E to PE, and they form a positive feedback loop. A similar positive feedback loop between TGF-β and partial EMT is proposed by Grande et al (Grande et al., 2015). Here we integrated these two positive feedback loops into one in our model since Wnt is necessary for TGF-β-mediated myofibroblast activation. Another positive feedback is formed between myofibroblast and Wnt, given that myofibroblast secrets Wnt while the latter promotes the transition of activated fibroblast to myofibroblast and the proliferation of myofibroblast. Taken together, the tubular module and fibroblast module secret cytokines that target themselves and each other through autocrine and paracrine mechanisms, resulting in an intertwined regulatory network.

Based on the information about the cell-cell communication, we constructed the following coarse-grained ODE model.

<u>ODE for the Tubular Module</u>

$$E' = -kd_{ei} * Insult * E + (k_{regeration0} + k_{regeration} * \frac{Wnt}{Wnt+J_{regeration}}) * E * 0 - \left(k_{ep1} * \frac{Wnt^2}{Wnt^2+J_{ep}^2}\right) * E + k_{pe} * PE + k_{repair} * \frac{Wnt}{Wnt+J_{repair}} * IE$$

$$IE' = kd_{ei} * Insult * E - k_{repair} * \frac{Wnt}{Wnt + J_{repair}} * IE - d_{IE} * IE$$

$$PE' = k_{ep1} * \frac{Wnt^2}{Wnt^2 + J_{ep}^2} * E - k_{pe} * PE$$

The tubular cell is injured under insult with a rate kd_{ei}. $O = 100 - E - IE - PE$ represents the percentage of dead tubular cells (or vacant tubular sites for new generated tubular cells). With a mean field approximation, the regeneration rate of tubular cells linearly depends on the percentage of the healthy tubular cells E and O. This rate expression is based on the following biological considerations. Only healthy tubular cell is proliferating while the partial EMT and injured tubular is under cell cycle arrest. Also the renal tissue has a size control mechanism to make sure the tissue will recover back to the normal size after regeneration. That is, a new tubular cell is generated only if there is a vacant site available. In addition to a basic regeneration with a rate $k_{regeration0}$, regeneration of tubular cell is promoted by Wnt, and is modeled to follow a Michaelis-Menten kinetics with a maximum $k_{regeration}$. Repair of injured tubular cells is promoted by Wnt, and is also modeled by a Michaelis–Menten kinetics with a maximum rate k_{repair}. Transition from a healthy tubular cell to the partial EMT state is promoted by Wnt, and is modeled with a Hill function with a maximum rate k_{ep1} and partial EMT tubular cell transits to tubular epithelial with a constant rate k_{pe}. Healthy and injured tubular cells also have their respective death rates, while partial EMT cells are protected from death (Vega et al., 2004).

ODE for secretion signals

$$Shh' = k_{Shh1} * IE + k_{Shh2} * PE - d_{Shh} * Shh$$

$$Wnt' = k_{win1} * PE + k_{win2} * Myo - d_{wnt} * Wnt$$

Both injured tubular cells and partial EMT tubular cells secrete Shh, while both PE and myofibroblast secrete Wnt. For simplicity we model the processes linearly.

ODE for the Tubular Module

$$Fib_r' = k_{fib0} - d_{fibr} * Fib_r - k_{fa1} * Shh * Fib_r - k_{fa2} * Wnt * Fib_r$$

$$\mathrm{Fib}_a' = k_{fa1} * \mathrm{Shh} * \mathrm{Fib}_r + k_{fa2} * \mathrm{Wnt} * \mathrm{Fib}_r - d_{fiba} * \mathrm{Fib}_a + \left(k_{fp1} * \frac{\mathrm{Shh}^2}{\mathrm{Shh}^2 + \mathrm{Jfp1}^2} + k_{fp2} * \frac{\mathrm{Wnt}^2}{\mathrm{Wnt}^2 + J_{fp2}^2}\right) * \mathrm{Fib}_a * \left(1 - \frac{\mathrm{Myo} + \mathrm{Fib}_a + \mathrm{Fib}_r}{M_{max}}\right) - k_{fm1} * \mathrm{Fib}_a * \frac{\mathrm{Shh}^2}{\mathrm{Shh}^2 + J_{fm1}^2} - k_{fm2} * \mathrm{Fib}_a * \frac{\mathrm{Wnt}^2}{\mathrm{Wnt}^2 + J_{fm2}^2} + k_{mf} * \mathrm{Myo}$$

$$\mathrm{Myo}' = k_{fm1} * \mathrm{Fib}_a * \frac{\mathrm{Shh}^2}{\mathrm{Shh}^2 + J_{fm1}^2} + k_{fm2} * \mathrm{Fib}_a * \frac{\mathrm{Wnt}^2}{\mathrm{Wnt}^2 + J_{fm2}^2} - k_{mf} * \mathrm{Myo} + k_m * \frac{\mathrm{Wnt}^2}{\mathrm{Wnt}^2 + J_m^2} * \mathrm{Myo} * \left(1 - \frac{\mathrm{Myo} + \mathrm{Fib}_a + \mathrm{Fib}_r}{M_{max}}\right) + k_{m2} * \mathrm{PE} - d_m * \mathrm{Myo}$$

Activation of fibroblasts linearly depends on both Shh and Wnt with rates k_{fa1} and k_{fa2} respectively. Proliferation of activated fibroblasts depends on Shh and Wnt, and is modeled by a Hill function with maximum rates k_{fp1} and k_{fp2} respectively, and a factor of vacant or available interstitial space for fibroblast and myofibroblasts (1- (Myo + Fib_a + Fib_r)/M_{max}), where M_{max} represents the maximal total level of Myofibroblasts and fibroblasts. Transition of activated fibroblast to myofibroblast depends on Shh and Wnt, which is modeled by a Hill function with maximum rates k_{fm1} and k_{fm2}, respectively. Proliferation of myofibroblast depends on Wnt and is modeled by a Hill function with maximum rates k_m. A basic myofibroblast generation from other possible recourses is assumed linearly regulated by PE. A linear death term is assumed for fibroblast and myofibroblast.

Due to lack of detailed information, in the above equations we use simple and generic mass action, Michaelis-Menten, and Hill function forms to model the kinetic processes. Our further numerical tests show that our main results of existence of four outcomes are largely insensitive to the exact forms of these terms or the parameters, and the key essential components are existence of the positive feedback loops with sufficient overall nonlinearity.

The level of myofibroblasts is one output of the model. Extensive and persistent activation of myofibroblasts induces excessive ECM accumulation and eventually leads to fibrosis. A complete resolution of myofibroblasts is an indicator of renal function recovery after damage. Table S1-2 provide the definition and values of the parameters and variables, respectively.

In our experiment, ischemia/reperfusion injury (IRI) is introduced to the mice for different periods from 10 min to 30 min to induce different levels of renal damage. In our model, the renal damage is introduced by a period of insults, which promotes normal epithelial tubular to injured

tubular cell with a rate constant $\mathrm{kd_{ei}}$. The strength of the insult for the simulation is set as 400 (in arbitrary unit, a.u.) except as indicated otherwise. To mimic the heterogeneity at the population level, values of the parameter set is randomly and uniformly chosen from 80 to 120% of default values with Latin Hypercubic sampling. Ward linkage is used for the hierarchical clustering analysis of the marker levels. To mimic the constant overexpression or downregulation of Wnt in Fig.4, the secretion rate of Wnt from myofibroblast was increased or decreased by 15%.

Parameter Estimation and Justification

Table S1-2 summarize all the model parameters. Here we discuss how we estimate and justify the parameters.

The doubling time of immortalized renal proximal tubular epithelial cells (RPTEC/TERT1) is about 96 hours (Wieser et al., 2008). Thus, the regeneration rate of immortalized RPTEC/TERT1 is about ln(2)/96 h^{-1} =0.007 h^{-1}. In the kidney without damage, most of tubular epithelial cells are in the quiescent state and thus the regeneration rate is much smaller. Thus, we assume a very small basic regeneration rate ($\mathrm{k_{regeration0}}$) for the healthy tubular epithelial cells. The regeneration rate is significantly increased after renal damage, and is dependent on the concentration of Wnt [6]. Therefore, we use a regeneration rate ($\mathrm{k_{regeration}}$) of healthy tubular cells mediated by Wnt much larger than the basic regeneration rate ($\mathrm{k_{regeration0}}$), but still smaller than the regeneration rate of immortalized tubular cells since not all of the tubular cells have exit quiescence. The repair rate of the injured cells ($\mathrm{k_{repair}}$) is set as 50-fold as the regeneration rate mediated by Wnt as we expect that the injured cell does not undergo the whole process of cell cycle and can be repaired quickly. The Michaelis constant of Wnt-dependent repair of damaged tubular ($\mathrm{J_{repair}}$) is set to be much smaller to the max level of Wnt as we assume that Wnt is critical for tubular cell repair (Tan et al., 2016). The death rate of injured tubular cells ($\mathrm{d_{IE}}$) is set 4-fold as the repair rate of injured tubular cells ($\mathrm{k_{repair}}$) since we assume that most of injured tubular cell is dead due to severe damage in different ways including apoptosis and regulated necrosis.

The rate of tubular cell injury depends on the insults, as different types of insults induce renal damage at different rates. Here, we mainly focus on Ischemia-Reperfusion Injury (IRI), which a major insult of AKI and induces tubular injury. The rate of tubular cell injury ($\mathrm{kd_{ei}}$) is estimated based on the percentage of the injured tubular cell can reach up to 20% at one day after IRI (Zhou et al., 2018).

Shh is mainly secreted by injured tubular cells and promotes the fibroblast proliferation and activation, but has no effect on the proliferation of tubular epithelial cells (Zhou et al., 2014). The secretion and degradation rates of Shh and Wnt have not been measured. Therefore, the secretion rates of Shh and Wnt ($k_{Shh1}, k_{win1}, k_{win2}$) are estimated based on the reports that Shh can be observed as early of 1h after IRI while Wnt can be observed at as early as 24 hours (Terada et al., 2003; Xiao et al., 2016). Here, we used a reduced unit for Shh and Wnt and set the degradation rates of Shh and Wnt (d_{Shh}, d_{wnt}) by scaling the maximum steady state level of Shh and Wnt to ~8. As most of the Shh is secreted by the injured tubular cell [17], we assume a rate (k_{Shh2}) for partial EMT tubular cells to secrete Shh smaller than that from injured tubular cells.

In our model, we explicitly considered two functions of Wnt on the tubular epithelial cell, promoting proliferation of healthy epithelial tubular cell and its transition to partial EMT state. In our previous reports (Tian et al., 2013; Zhang et al., 2014), the partial EMT is stable yet reversible as it is governed by a reversible bistable switch. Reversibility of partial EMT is also supported by a recent experimental report in the renal system, in which Snail1 inhibition promotes the reversion of the partial EMT tubular to epithelial phenotype and increase of proliferation (Grande et al., 2015). Given the maximum steady-state levels of Wnt is ~ 8, we set the Michaelis constant of Wnt-dependent partial EMT (J_{ep}) to be 7, the Michaelis constant of Wnt-dependent regeneration of healthy tubular ($J_{regeration}$) to be 5. That is, the Wnt concentration required to activate regeneration is lower than that of inducing partial EMT. These choices are consistent with the observation that under mild injury the percentage of cells under cycle arrest (including partial EMT tubular cells) is low(Yang et al., 2010). The dilated renal tubular epithelium, consisting of partial EMT tubular cells, can be already observed from 1 day after UUO (Li et al., 2007). We expect that the AKI-induced partial EMT has similar dynamics, and set the transition rate from healthy tubular cells to partial EMT tubular k_{ep1} = 0.11 h^{-1}. Considering that it is a functional requirement for the system to efficiently reverse partial EMT for renal tubular cells after completion of repair, we set the transition rate from partial EMT tubular cells to healthy tubular (k_{pe}) to be 4.5-fold of k_{ep1}.

Without injury, there is a very low density of resident fibroblasts in the interstitial space between nephrons (Strutz and Zeisberg, 2006). Shh and Wnt significantly increase the proliferation rate of fibroblasts. Therefore we set values of the basic production rate and basic death rate of resident fibroblasts as smaller than its production rate mediated by Shh and Wnt. Also, the steady state level of resident fibroblasts is determined by the ratio of its basic production rate

and basic death rate ($k_{fib0}/d_{fib0} = 1$), to give a ratio of resident fibroblasts to tubular epithelial cells 1:100. The activation rates of fibroblasts (k_{fa1}, k_{fa2}) are estimated based on the rapid activation of fibroblast after AKI (Rognoni et al., 2018). The basic death rate of the activated fibroblast ($\mathrm{d_{fiba}}$) is set to be the same as that of resident fibroblast ($\mathrm{d_{fib}}$) as there is no evidence that the activation changes its death rate. The proliferation rate of activated fibroblast is increased as it is promoted by Shh and Wnt (Sörensen et al., 2011). Michaelis constants of Shh-dependent and Wnt-dependent proliferation of fibroblasts ($\mathrm{J_{fm1}}, \mathrm{J_{fm2}}$) are assumed to be similar to the Michaelis constant of Wnt-dependent regeneration of healthy tubular cells ($J_{regeration}$). The doubling time of activated fibroblast is about 24h, thus its proliferation rate is about ln(2)/24h = 0.029/h. Here, we use rather larger production rates for fibroblasts and myofibroblast ($\mathrm{k_{fp1}}, \mathrm{k_{fp2}}, \mathrm{k_m}$) since in addition to proliferation there are multiple other sources of activated fibroblast and myofibroblast, including pericyte, fibrocyte, endothelial cells and tubular cell (Grande and Lopez-Novoa, 2009; Liu, 2011). The contribution of full EMT program to the production of myofibroblast is very limited compared with other source and most the tubular cells in the partial EMT state stay in the original site rather be further transited to mesenchymal state (Grande et al., 2015; LeBleu et al., 2013). We also set the Michaelis constant of Wnt-dependent production of myofibroblast ($\mathrm{J_{fm2}}$) to be smaller than other Michaelis constants to account for contributions from multiple sources of myofibroblast that are not explicitly considered in the model. Death of activated fibroblast and myofibroblast is actively through matrix metalloproteinase (MMP-7) induced FasL for fast resolution after the renal damage is repaired (Zhou et al., 2013b). Here, the regulation of myofibroblast apoptosis is not explicitly considered in the model but we set a rather large death rate ($\mathrm{d_m}$) to show this programmed death of myofibroblast. The maximum level of the interstitial cells (M_{max}) in the condition of fibrosis is less than the maximum level of the tubular cell but is significantly increased from the basic level of the resident fibroblast. We assumed a 60-fold increase for the possible maximum level of the interstitial cell. The transition rates between fibroblast and myofibroblast have not been measured. Here we assume the transition rate from fibroblast to myofibroblast ($\mathrm{k_{fm1}}, \mathrm{k_{fm2}}$) is much larger than the transition rate from myofibroblast to fibroblast ($\mathrm{k_{mf}}$) as the majority of activated fibroblast is transited to myofibroblast for the tissue repair (Grande and Lopez-Novoa, 2009). Because Shh is the most important cytokine that promotes differentiation of fibroblasts into myofibroblasts (Ding et al., 2012), the Michaelis constant of Shh-dependent fibroblast to myofibroblast ($\mathrm{J_{fm1}}$) is set much smaller than the Michaelis constant of Wnt-dependent fibroblast to myofibroblast ($\mathrm{J_{fm2}}$).

Overall, we estimated all the parameters either directly from the literature, or the relative relationship between parameters based on the existing reports as stated above, together with fitting the dynamics of the key regulators and the overall dependence of the renal outcomes on the insult (IRI) duration. In addition, because of heterogeneity among individuals, all the parameters have a variation. We mimicked this heterogeneity in our simulations by choosing values of the parameter set randomly and uniformly from 80 to 120% of default values with Latin Hypercubic sampling.

The fate of organism death in the mathematical model. Our mathematical model does not treat the complex process of organism death explicitly. Instead we used the cumulative sum of dead tubular cell (O) ($\int_{t=0}^{t=30day} Odt$) as an indicator of death by considering that the death is induced by death-inducing factors leaked at the sites of dead tubular cells. During the repair process there is constant tubular cell death and replenishment from healthy tubular cells. Therefore, the cumulative sum of the net vacant tubular sites, but not the individual cell death, is relevant to the death risk of the organ and the organism. As shown in Supplementary Figure 2A, a mouse assumes a fate of death without further simulation (Red line) if the cumulative sum of dead tubular cell is larger than a threshold value (Cumsum_θ=50). In contrast, in the case where $\mathrm{Cumsum} < \mathrm{Cumsum}_\theta$, the recovery can be continued (green line).

Procedure of searching the optimal dynamic Treatment Design for AKI by Targeting on Wnt

In order to find the optimal treatment design for AKI, the following procedure is used.

1. For each drug ($\mathrm{Drug_i}$), we have three parameters, the dose ($\mathrm{Dose_i}$), the duration ($\mathrm{Dura_i}$), and the timing ($\mathrm{T_i}$) that determine how much, how long and when this drug is applied.
2. A score function is defined to quantify the effectiveness of the treatment design. Here, we considered the organism death risk, fibrosis risk, the duration of drugs and the recovery time and used this score function,

$$\mathrm{Score_{therapy}} = \lambda_1 * \mathrm{Risk_{Death}} + \lambda_2 * \mathrm{Risk_{Fibrosis}} + \lambda_3 * \mathrm{RecTime} + \sum_{i=4}^{4+n} \lambda_i * \mathrm{Dura_i}$$

where $(\lambda_1 > \lambda_2 > \lambda_3 = \lambda_4 = \cdots = \lambda_{4+n})$.

$\mathrm{Risk_{Death}}$ ($= \frac{1}{\mathrm{Cumsum}_\theta} \int_{t=0}^{t=30\ days} O\ dt$ is evaluated as the cumulative sum of dead tubular cells normalized by Cumsum_θ, which can be considered as the total level of death-inducing factors leaked by dead tubular cells. $\mathrm{Risk_{Fibrosis}}$ ($= \frac{1}{Myo_m} \int_{t=0}^{t=30\ days} Myo\ dt$) is

evaluated as the cumulative sum of myofibroblast level normalized by the maximum level of myofibroblast at MARS state Myo_m, which can be considered as the total level of extracellular matrix (ECM) generated by myofibroblasts. That is, both a transient high level and a sustained low level of myofibroblasts increase the risk of fibrosis. $\mathrm{RecTime}$ is the time point when the myofibroblast level is reduced below the threshold of the transition from PARS and iPARS (set as 1 here). It assumes a maximum value of 30 days if the level of myofibroblasts does not go below the threshold value at the end of the simulation (30 days).

The weight of death risk λ_1 is set to be much larger than that of fibrosis risk λ_2, and the latter is much larger than that of recovery time λ_3 and the duration of drugs λ_i. The reason for this setting is that the top priority of a treatment plan is life-saving and the second priority is risk reduction of fibrosis, and a fast recovery and a minimized medicine usage at the last.

3. Search the optimal therapy design in the parameter space with Metropolis algorithm. Here, we have two drugs targeting on Wnt, Wnt and inhibitor, thus we can have a 6-dimensional space.
    a. Set the initial temperature T to some high value.
    b. Choose an initial treatment design as $\mathrm{Design}_0 = [\mathrm{T1}, \mathrm{Dose1}, \mathrm{Dur1}, \mathrm{T2}, \mathrm{Dose2}, \mathrm{Dur2}]$ and calculate its therapy score, Score_0.
    c. Generate a new treatment design $\mathrm{Design}_1 = \mathrm{Design}_0 + \varepsilon * \Delta\mathrm{Design}$, where $\Delta\mathrm{Design}$ specifies the displacement per step and ε is a vector of random integer with (-1 0 1).
    d. Calculate the therapy score Score_1 with the current treatment design Design1.
    e. Calculate the acceptance probability $\mathrm{p} = e^{-(\mathrm{Score}_1 - \mathrm{Score}_0)/\mathrm{T}}$. Generate a random number γ_1 from with uniform distribution between 0 and 1. Update $\mathrm{Design}_0 = \mathrm{Design}_1$ if $\gamma_1 < \mathrm{p}$. Otherwise, reject the step k to k+1.
    f. Reduce the temperature T=T-ΔT. ΔT is a small number.
    g. Update k. If k is larger than a maximum step number, stop. Otherwise return to step a.

It is noted that our searching algorithm can start from any initial treatment design set. Our simulation started from no treatment with $\mathrm{Design}_0 = [0, 0, 0, 0, 0, 0]$. The Metropolis algorithm guided the search to treatment designs with drugs added. *The weight* of different factor [$\lambda 1$ $\lambda 2$ $\lambda 3$ $\lambda 4$ $\lambda 5$] in score function *is set as* [500 10 1 1 1] in Figure 5.

Supplemental References:

Akhmetshina, A., Palumbo, K., Dees, C., Bergmann, C., Venalis, P., Zerr, P., Horn, A., Kireva, T., Beyer, C., Zwerina, J.*, et al.* (2012). Activation of canonical Wnt signalling is required for TGF-β-mediated fibrosis. Nat Commun *3*, 735.

Belayev, L.Y., and Palevsky, P.M. (2014). The link between acute kidney injury and chronic kidney disease. Curr Opin Nephrol Hypertens *23*, 149-154.

Bonventre, J.V. (2002). Kidney ischemic preconditioning. Curr Opin Nephrol Hypertens *11*, 43-48.

Dai, C., Yang, J., and Liu, Y. (2002). Single injection of naked plasmid encoding hepatocyte growth factor prevents cell death and ameliorates acute renal failure in mice. J Am Soc Nephrol *13*, 411-422.

Ding, H., Zhou, D., Hao, S., Zhou, L., He, W., Nie, J., Hou, F.F., and Liu, Y. (2012). Sonic hedgehog signaling mediates epithelial-mesenchymal communication and promotes renal fibrosis. J Am Soc Nephrol *23*, 801-813.

Grande, M.T., and Lopez-Novoa, J.M. (2009). Fibroblast activation and myofibroblast generation in obstructive nephropathy. Nat Rev Nephrol *5*, 319-328.

Grande, M.T., Sanchez-Laorden, B., Lopez-Blau, C., De Frutos, C.A., Boutet, A., Arevalo, M., Rowe, R.G., Weiss, S.J., Lopez-Novoa, J.M., and Nieto, M.A. (2015). Snail1-induced partial epithelial-to-mesenchymal transition drives renal fibrosis in mice and can be targeted to reverse established disease. Nat Med *21*, 989-997.

Hao, S., He, W., Li, Y., Ding, H., Hou, Y., Nie, J., Hou, F.F., Kahn, M., and Liu, Y. (2011). Targeted inhibition of beta-catenin/CBP signaling ameliorates renal interstitial fibrosis. J Am Soc Nephrol *22*, 1642-1653.

Joo, J.D., Kim, M., D'Agati, V.D., and Lee, H.T. (2006). Ischemic Preconditioning Provides Both Acute and Delayed Protection against Renal Ischemia and Reperfusion Injury in Mice. J Am Soc Nephrol *17*, 3115-3123.

Kuncewitch, M., Yang, W.L., Corbo, L., Khader, A., Nicastro, J., Coppa, G.F., and Wang, P. (2015). WNT Agonist Decreases Tissue Damage and Improves Renal Function After Ischemia-Reperfusion. Shock *43*, 268-275.

LeBleu, V.S., Taduri, G., O'Connell, J., Teng, Y., Cooke, V.G., Woda, C., Sugimoto, H., and Kalluri, R. (2013). Origin and function of myofibroblasts in kidney fibrosis. Nat Med *19*, 1047-1053.

Leung, K.C.W., Tonelli, M., and James, M.T. (2013). Chronic kidney disease following acute kidney injury[mdash]risk and outcomes. Nat Rev Nephrol *9*, 77-85.

Li, B., Lang, X., Cao, L., Wang, Y., Lu, Y., Feng, S., Yang, Y., Chen, J., and Jiang, H. (2017). Effect of remote ischemic preconditioning on postoperative acute kidney injury among patients undergoing cardiac and vascular interventions: a meta-analysis. J Nephrol *30*, 19-33.

Li, Y., Yang, J., Luo, J.H., Dedhar, S., and Liu, Y. (2007). Tubular epithelial cell dedifferentiation is driven by the helix-loop-helix transcriptional inhibitor Id1. J Am Soc Nephrol *18*, 449-460.

Liu, Y. (2011). Cellular and molecular mechanisms of renal fibrosis. Nat Rev Nephrol *7*, 684-696.

Lovisa, S., LeBleu, V.S., Tampe, B., Sugimoto, H., Vadnagara, K., Carstens, J.L., Wu, C.C., Hagos, Y., Burckhardt, B.C., Pentcheva-Hoang, T.*, et al.* (2015). Epithelial-to-mesenchymal transition induces cell cycle arrest and parenchymal damage in renal fibrosis. Nat Med *21*, 998-1009.

Maarouf, O.H., Aravamudhan, A., Rangarajan, D., Kusaba, T., Zhang, V., Welborn, J., Gauvin, D., Hou, X., Kramann, R., and Humphreys, B.D. (2016). Paracrine Wnt1 Drives Interstitial Fibrosis without Inflammation by Tubulointerstitial Cross-Talk. J Am Soc Nephrol *27*, 781-790.

Nelson, W.J., and Nusse, R. (2004). Convergence of Wnt, beta-catenin, and cadherin pathways. Science *303*, 1483-1487.

Park, K.M., Byun, J.Y., Kramers, C., Kim, J.I., Huang, P.L., and Bonventre, J.V. (2003). Inducible nitric-oxide synthase is an important contributor to prolonged protective effects of ischemic preconditioning in the mouse kidney. J Biol Chem *278*, 27256-27266.
Park, K.M., Chen, A., and Bonventre, J.V. (2001). Prevention of kidney ischemia/reperfusion-induced functional injury and JNK, p38, and MAPK kinase activation by remote ischemic pretreatment. J Biol Chem *276*, 11870-11876.
Rognoni, E., Pisco, A.O., Hiratsuka, T., Sipila, K.H., Belmonte, J.M., Mobasseri, S.A., Philippeos, C., Dilao, R., and Watt, F.M. (2018). Fibroblast state switching orchestrates dermal maturation and wound healing. Mol Syst Biol *14*, e8174.
Sörensen, I., Susnik, N., Inhester, T., Degen, J.L., Melk, A., Haller, H., and Schmitt, R. (2011). Fibrinogen, acting as a mitogen for tubulointerstitial fibroblasts, promotes renal fibrosis. Kidney Int *80*, 1035-1044.
Strutz, F., and Zeisberg, M. (2006). Renal Fibroblasts and Myofibroblasts in Chronic Kidney Disease. J Am Soc Nephrol *17*, 2992-2998.
Tan, R.J., Zhou, D., and Liu, Y. (2016). Signaling Crosstalk between Tubular Epithelial Cells and Interstitial Fibroblasts after Kidney Injury. Kidney Dis *2*, 136-144.
Terada, Y., Tanaka, H., Okado, T., Shimamura, H., Inoshita, S., Kuwahara, M., and Sasaki, S. (2003). Expression and function of the developmental gene Wnt-4 during experimental acute renal failure in rats. J Am Soc Nephrol *14*, 1223-1233.
Tian, X.J., Zhang, H., and Xing, J. (2013). Coupled reversible and irreversible bistable switches underlying TGFβ-induced epithelial to mesenchymal transition. Biophys J *105*, 1079-1089.
Vega, S., Morales, A.V., Ocaña, O.H., Valdés, F., Fabregat, I., and Nieto, M.A. (2004). Snail blocks the cell cycle and confers resistance to cell death. Genes Dev *18*, 1131-1143.
Wieser, M., Stadler, G., Jennings, P., Streubel, B., Pfaller, W., Ambros, P., Riedl, C., Katinger, H., Grillari, J., and Grillari-Voglauer, R. (2008). hTERT alone immortalizes epithelial cells of renal proximal tubules without changing their functional characteristics. Am J Physiol Renal Physiol *295*, F1365-1375.
Xiao, L., Xu, B., Zhou, L., Tan, R.J., Zhou, D., Fu, H., Li, A., Hou, F.F., and Liu, Y. (2019). Wnt/beta-catenin regulates blood pressure and kidney injury in rats. Biochim Biophys Acta Mol Basis Dis *1865*, 1313-1322.
Xiao, L., Zhou, D., Tan, R.J., Fu, H., Zhou, L., Hou, F.F., and Liu, Y. (2016). Sustained Activation of Wnt/beta-Catenin Signaling Drives AKI to CKD Progression. J Am Soc Nephrol *27*, 1727-1740.
Yang, L., Besschetnova, T.Y., Brooks, C.R., Shah, J.V., and Bonventre, J.V. (2010). Epithelial cell cycle arrest in G2/M mediates kidney fibrosis after injury. Nat Med *16*, 535-543.
Zarbock, A., Schmidt, C., Van Aken, H., Wempe, C., Martens, S., Zahn, P.K., Wolf, B., Goebel, U., Schwer, C.I., Rosenberger, P.*, et al.* (2015). Effect of remote ischemic preconditioning on kidney injury among high-risk patients undergoing cardiac surgery: a randomized clinical trial. Jama *313*, 2133-2141.
Zhang, J., Tian, X.J., Zhang, H., Teng, Y., Li, R., Bai, F., Elankumaran, S., and Xing, J. (2014). TGF-beta-induced epithelial-to-mesenchymal transition proceeds through stepwise activation of multiple feedback loops. Sci Signal *7*, ra91.
Zhou, D., Fu, H., Xiao, L., Mo, H., Zhuo, H., Tian, X., Lin, L., Xing, J., and Liu, Y. (2018). Fibroblast-Specific beta-Catenin Signaling Dictates the Outcome of AKI. J Am Soc Nephrol *29*, 1257-1271.
Zhou, D., Li, Y., Lin, L., Zhou, L., Igarashi, P., and Liu, Y. (2012). Tubule-specific ablation of endogenous beta-catenin aggravates acute kidney injury in mice. Kidney Int *82*, 537-547.
Zhou, D., Li, Y., Zhou, L., Tan, R.J., Xiao, L., Liang, M., Hou, F.F., and Liu, Y. (2014). Sonic hedgehog is a novel tubule-derived growth factor for interstitial fibroblasts after kidney injury. J Am Soc Nephrol *25*, 2187-2200.

Zhou, D., Tan, R.J., Fu, H., and Liu, Y. (2016). Wnt/β-catenin signaling in kidney injury and repair: a double-edged sword. Lab Invest *96*, 156-167.
Zhou, D., Tan, R.J., Lin, L., Zhou, L., and Liu, Y. (2013a). Activation of hepatocyte growth factor receptor, c-met, in renal tubules is required for renoprotection after acute kidney injury. Kidney Int *84*, 509-520.
Zhou, D., Tan, R.J., Zhou, L., Li, Y., and Liu, Y. (2013b). Kidney tubular β-catenin signaling controls interstitial fibroblast fate via epithelial-mesenchymal communication. Sci Rep *3*, 1878.
Zhou, L., Li, Y., Hao, S., Zhou, D., Tan, R.J., Nie, J., Hou, F.F., Kahn, M., and Liu, Y. (2015). Multiple genes of the renin-angiotensin system are novel targets of Wnt/beta-catenin signaling. J Am Soc Nephrol *26*, 107-120.